NORSAR

ROYAL NORWEGIAN COUNCIL FOR SCIENTIFIC AND INDUSTRIAL RESEARCH

Scientific Report No. 2-82/83

SEMIANNUAL TECHNICAL SUMMARY

1 October 1982 – 31 March 1983

Linda B. Tronrud (ed.)

Kjeller, June 1983

SECURITY CLASSIFICATION OF THIS PAGE (When Data Entered)

REPORT DOCUMENTATION PAGE		READ INSTRUCTIONS BEFORE COMPLETING FORM
1. REPORT NUMBER F08606-79-C-0001	2. GOVT ACCESSION NO.	3. RECIPIENT'S CATALOG NUMBER
4. TITLE (and Subtitle) SEMIANNUAL TECHNICAL SUMMARY 1 October 1982 - 31 March 1983		5. TYPE OF REPORT & PERIOD COVERED 1 Oct 82 - 31 Mar 83
		6. PERFORMING ORG. REPORT NUMBER Sci. Report 2-82/83
7. AUTHOR(s) L.B. Tronrud (ed.)		8. CONTRACT OR GRANT NUMBER(s)
9. PERFORMING ORGANIZATION NAME AND ADDRESS NTNF/NORSAR Post Box 51 N-2007 Kjeller, Norway		10. PROGRAM ELEMENT, PROJECT, TASK AREA & WORK UNIT NUMBERS NORSAR Phase 3
11. CONTROLLING OFFICE NAME AND ADDRESS AFTAC/HQ/TGX Patrick AFB FL 32925 USA		12. REPORT DATE June 1983
		13. NUMBER OF PAGES 88
14. MONITORING AGENCY NAME & ADDRESS(if different from Controlling Office)		15. SECURITY CLASS. (of this report)
		15a. DECLASSIFICATION/DOWNGRADING SCHEDULE
16. DISTRIBUTION STATEMENT (of this Report) APPROVED FOR PUBLIC RELEASE; DISTRIBUTION UNLIMITED.		
17. DISTRIBUTION STATEMENT (of the abstract entered in Block 20, if different from Report)		
18. SUPPLEMENTARY NOTES		
19. KEY WORDS (Continue on reverse side if necessary and identify by block number)		
20. ABSTRACT (Continue on reverse side if necessary and identify by block number)		

DD FORM 1 JAN 73 1473 EDITION OF 1 NOV 65 IS OBSOLETE

SECURITY CLASSIFICATION OF THIS PAGE (When Data Entered)

This report describes the operation, maintenance and research activities at the Norwegian Seismic Array (NORSAR) for the period 1 October 1982 to 31 March 1983.

The uptime of the NORSAR online detection processor system has averaged 95.7%, as compared to 92.3 for the previous period. Most of the downtime was caused by CPU and disk drive problems. A total of 1208 events were reported in this period, giving a daily average of 6.6 events. The number of reported events per month varies from 144 in November to 268 in March. There have been some difficulties with the communications lines; 06C was down at the beginning of the period due to a seriously damaged cable which was finally repaired 3 November. All communications circuits were turned off 12 December in connection with dismantling/removal of the SPS. There were also some difficulties with the telemetry stations at 02B due to snow and ice reducing the charging effect of the solar cells.

The DP system implemented on IBM 4331/MODCOMP is described in Section III. Programs and operational routines used on the SPS-system have been converted. Graphic displays are now used in array monitoring routines. A data-loss problem caused by sharing of disk between the IBM 4331 and 4341 has been corrected, and during the second half of the reporting period, the shared-disk principle was instigated for programs as well. A synchronization problem in the MODCOMP system has been corrected by restarting and resynchronizing the system twice a week.

Section IV describes field instrumentation and maintenance activities at the NORSAR Maintenance Center.

The research activity is briefly described in Section VI. Subsection 1 discusses the absorption band effect on long-period body waves. Subsection 2 discusses the present seismic evidence for a boundary layer at the base of the mantle. Subsection 3 presents the effect of aliasing on the NORSAR detector performance. Subsection 4 presents results of a study of seismic noise at high frequencies. Subsection 5 discusses power spectral bias sources and quantization levels. In subsection 6 the results of a study of magnitudes from P coda and Lg using NORSAR data are presented. Subsection 7 discusses the design work for a new regional array in Norway.

AFTAC Project Authorization No.	:	VELA VT/0702/B/PMP, Amendment 1
ARPA Order No.	:	2551
Program Code No.	:	0F10
Name of Contractor	:	Royal Norwegian Council for Scientific and Industrial Research
Effective Date of Contract	:	1 October 1979
Contract Expiration Date	:	30 September 1983
Project Manager	:	Frode Ringdal (02) 71 69 15
Title of Work	:	The Norwegian Seismic Array (NORSAR) Phase 3
Amount of Contract	:	$4.762.383
Contract Period Covered by the Report	:	1 October 1982 - 31 March 1983

This research was supported by the Advanced Research Projects Agency of the Department of Defense and was monitored by AFTAC, Patrick AFB FL 32925, under contract no. F08606-79-C-0001.

NORSAR Contribution No. 334

TABLE OF CONTENTS

I. SUMMARY

This report describes the operation, maintenance and research activities at the Norwegian Seismic Array (NORSAR) for the period 1 October 1982 to 31 March 1983.

The uptime of the NORSAR online detection processor system has averaged 95.7%, as compared to 92.3 for the previous period. Most of the downtime was caused by CPU and disk drive problems. A total of 1208 events were reported in this period, giving a daily average of 6.6 events. The number of reported events per month varies from 144 in November to 268 in March. There have been some difficulties with the communications lines; 06C was down at the beginning of the period due to a seriously damaged cable which was finally repaired 3 November. All communications circuits were turned off 12 December in connection with dismantling/removal of the SPS. There were also some difficulties with the telemetry stations at 02B due to snow and ice reducing the charging effect of the solar cells.

The DP system implemented on IBM 4331/MODCOMP is described in Section III. Programs and operational routines used on the SPS-system have been converted. Graphic displays are now used in array monitoring routines. A data-loss problem caused by sharing of disk between the IBM 4331 and 4341 has been corrected, and during the second half of the reporting period, the shared-disk principle was instigated for programs as well. A synchronization problem in the MODCOMP system has been corrected by restarting and resynchronizing the system twice a week.

Section IV describes field instrumentation and maintenance activities at the NORSAR Maintenance Center.

The research activity is briefly described in Section VI. Subsection 1 discusses the absorption band effect on long-period body waves. Subsection 2 discusses the present seismic evidence for a boundary layer at the base of the mantle. Subsection 3 presents the effect of aliasing on the NORSAR detector performance. Subsection 4 presents results of a study of seismic noise at high frequencies. Subsection 5 discusses power spectral bias sources and quantization levels. In subsection 6 the results of a study of magnitudes from P coda and Lg using NORSAR data are presented. Subsection 7 discusses the design work for a new regional array in Norway.

II. OPERATION OF ALL SYSTEMS

II.1 Detection Prccessor (DP) Operation

There have been 61 breaks in the otherwise continuous operation of the NORSAR online system within the current 6-month reporting interval. Almost half of the downtime in this period was caused by a cut of the main power due to installation of a new transformer. Most of the stops due to DP software occurred in the first half of the period; the last month had only 3 stops. The uptime percentage for the period is 95.7 per cent as compared to 92.3 for the previous period.

Fig. II.1.1 and the accompanying Table II.1.1 both show the daily DP downtime for the days between 1 October 1982 and 31 March 1983. The monthly recording times and percentages are given in Table II.1.2.

The breaks can be grouped as follows:

a)	Stops related to possible program errors	51
b)	Maintenance stops	2
c)	Power breaks	6
d)	Hardware problems	2

The total downtime for the period was 185 hours and 50 minutes. The mean-time-between-failures (MTBF) was 2.9 days as compared with 1.4 days for the previous period.

J. Torstveit

LIST OF BREAKS IN DP PROCESSING THE LAST HALF-YEAR

DAY	START		STOP		COMMENTS.....
277	10	17	11	20	DP SOFTWARE
278	8	57	9	0	DP SOFTWARE
278	9	46	9	53	DP SOFTWARE
278	12	30	14	51	DP SOFTWARE
279	12	8	13	2	DP SOFTWARE
280	11	21	11	51	DP SOFTWARE
281	12	31	12	45	DP SOFTWARE
283	7	47	8	7	DP SOFTWARE
287	12	42	14	16	DP SOFTWARE
288	4	0	8	1	MODCOMP FAILURE
288	9	13	9	55	DP SOFTWARE
291	9	37	10	30	POWER BREAK
292	12	16	13	45	POWER BREAK
293	9	21	11	40	POWER BREAK
302	14	28	14	31	DP SOFTWARE
305	9	34	9	44	DP SOFTWARE
306	7	49	13	45	DP SOFTWARE
307	12	19	13	38	DP SOFTWARE
314	10	18	10	20	DP SOFTWARE
314	11	46	11	48	DP SOFTWARE
315	11	53	11	56	DP SOFTWARE
315	12	0	14	43	DP SOFTWARE
316	13	35	13	45	DP SOFTWARE
319	6	30	7	16	DP SOFTWARE
323	13	0	24	0	WORK ON MAIN POWER
324	0	0	24	0	--------//--------
325	0	0	24	0	--------//--------
326	0	0	9	20	--------//--------
333	8	38	9	52	POWER BREAK
334	3	39	8	14	DP SOFTWARE
334	13	9	13	16	DP SOFTWARE
334	19	57	20	15	DP SOFTWARE
334	21	27	24	0	DP SOFTWARE
335	0	0	7	16	DP SOFTWARE
335	8	33	9	57	DP SOFTWARE
335	13	52	13	55	DP SOFTWARE
336	8	48	9	11	DP SOFTWARE
340	13	10	13	40	DP SOFTWARE
346	8	25	11	40	DP SOFTWARE
354	12	0	14	51	DP SOFTWARE
357	8	17	8	42	DP SOFTWARE
357	19	49	21	1	DP SOFTWARE
361	8	14	12	39	DP SOFTWARE
361	12	39	14	35	CE MAINTENANCE
364	13	8	19	4	DP SOFTWARE
364	20	38	20	45	DP SOFTWARE
365	9	0	10	34	CE MAINTENANCE
1	12	37	12	59	DP SOFTWARE
6	8	36	9	4	DP SOFTWARE
7	9	38	9	47	DP SOFTWARE
7	10	16	10	19	DP SOFTWARE
13	7	54	8	15	DP SOFTWARE
17	12	38	14	24	DP SOFTWARE
17	16	6	19	37	DP SOFTWARE
18	8	9	13	45	DP SOFTWARE
20	3	34	7	31	DP SOFTWARE
21	0	49	9	22	OTHER SOFTWARE
21	11	24	13	5	CE HARDWARE
40	10	24	11	4	DP SOFTWARE
46	10	43	11	36	WORK ON MAIN POWER
57	6	0	13	17	DISK PROBLEM
58	10	22	13	44	DP SOFTWARE
58	19	15	23	23	DP SOFTWARE
66	13	48	14	8	DP SOFTWARE
76	13	38	14	1	DP SOFTWARE
77	10	0	16	13	DP SOFTWARE

Table II.1.1 List of breaks in DP processing in the period 1 Oct 82 - 31 Mar 83.

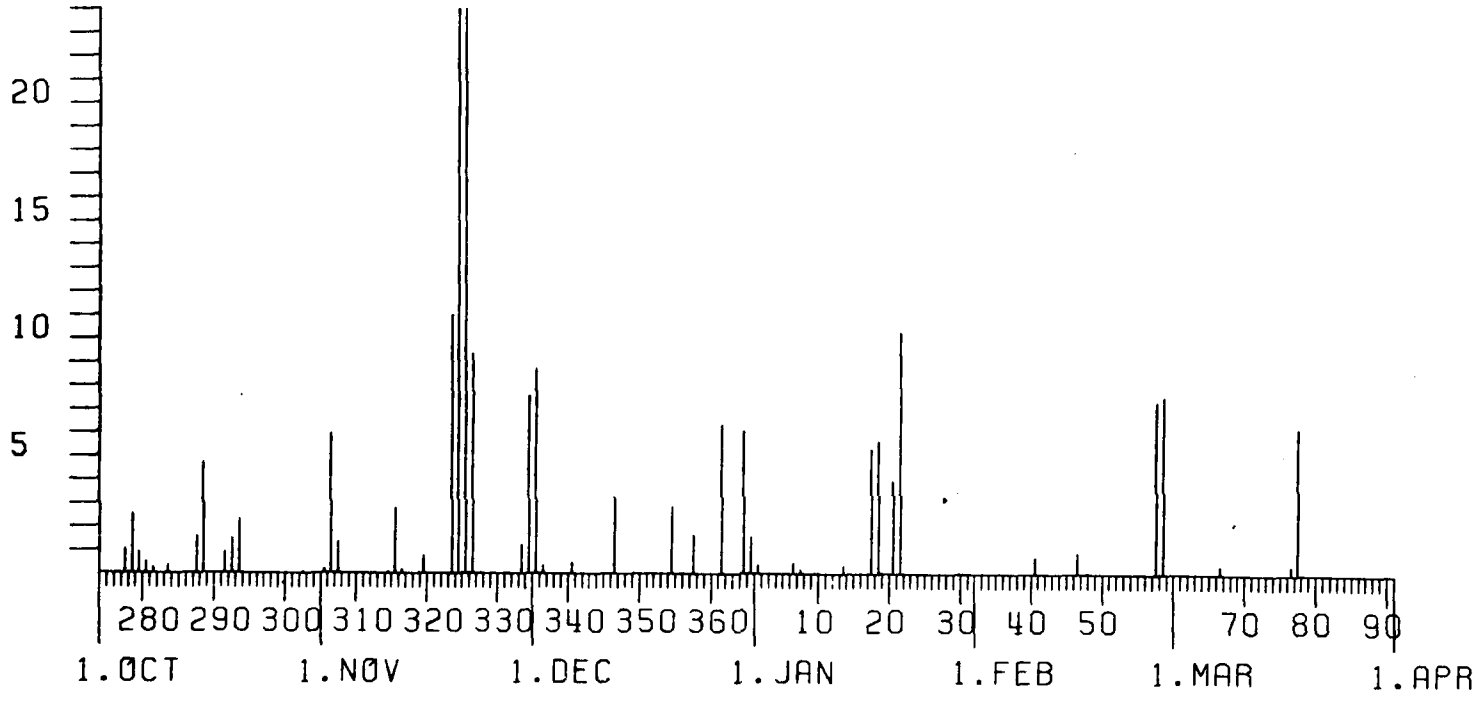

Fig. II.1.1 Detection Processor downtime in the period 1 Oct 82 - 31 March 83.

Month	DP Uptime (hrs)	DP Uptime (%)	No. of DP Breaks	No. of Days with Breaks	DP MTBF* (days)
Oct	727.47	97.8	15	12	1.9
Nov	635.70	87.7	14	13	1.8
Dec	717.72	95.8	13	9	2.3
Jan	717.57	96.4	11	8	2.5
Feb	703.68	97.6	5	4	4.6
Mar	737.08	99.1	3	3	7.7
	4239.22	95.7	61	49	2.9

*Mean-time-between-failures = (Total uptime/No. of up intervals)

TABLE II.1.2

Online System Performance
1 October 1982 - 31 March 1983

II.2 Event Processor Operation

In Table II.2.1 some monthly statistics of the Event Processor operation are given:

	Teleseismic	Core Phases	Sum	Daily
Oct 82	152	43	195	6.2
Nov 82	107	37	144	4.8
Dec 82	124	40	164	5.3
Jan 83	185	33	218	7.0
Feb 83	183	36	219	7.8
Mar 83	238	30	268	8.6
	989	219	1208	6.6

TABLE II.2.1

B. Kr. Hokland

II.3 Array Communication

Table II.3.1 reflects the performance of the communications system throughout the reporting period.

As also previously stated, the table not only reflects irregularities in the communication systems itself, but in addition also reflects other prominent conditions such as:

- CTV power failure
- Line switching during program debugging/corrections (at the NDPC)
- Maintenance visits
- NDPC-initiated tests
- MODCOMP resynchronization.

Since 21 September 1982 the MODCOMP Communications Processor has replaced the SPS.

Summary

October: 06C, which had been down since week 38/82, was still out of operation by end of October due to seriously damaged cable

November: 06C resumed operation (3 Nov). A few resynch. problems observed in connection with 01B in the beginning of November; otherwise, reliable system operation.

December: 12 Dec all communications circuits were turned off in connection with SPS dismantling/removal. Due to power line damage in the 02B area (11 Dec), this subarray was out of operation the remaining days of December in spite of strong efforts from the local power plant's crew.

January: Power back in the 02B area (4 Jan), but due to SLEM trouble, the subarray resumed operation 5 Jan. Found spikes in the 02C data (25 Jan), and this initiated a test and investigation period where telestations at Lillestrøm, Hamar and Lillehamer were involved.

February: After 9 Feb the 02C system was back in operation.

March: Between 5 and 11 Mar the 03C communications system was out of operation due to NTA cable work in the Rena area. 06C lost synchronization a number of times weeks 10-13.

Table II.3.2 indicates distribution of outages with respect to the individual subarrays.

Miscellaneous

Problems occurred in connection with 02B telemetry stations 11 Dec due to snow problems reducing the charging effect of the solar cells to the batteries. Operation resumed 27 Dec. The same problem occurred in January (10-14), but this time only telemetry station 04 was involved.

O.A. Hansen

Sub-Array	OCT (4) (4-31.10)		NOV (4) (1-28.11)		DEC (5) (29.11-2.1.83)		JAN (4) (3.1-30.1)		FEB (4) (31.1-27.2)		MAR (5) (28.2-3.4)		AVERAGE ½ YEAR	
	>20	>200	>20	>200	>20	>200	>20	>200	>20	>200	>20	>200	>20	>200
01A	0.3	-	0.2	1.8	1.3	-	0.9	-	0.8	-	1.1	-	0.7	0.3
01B	0.2	-	0.6	1.8	1.4	-	1.0	-	0.8	-	1.1	-	0.8	0.3
02B	0.3	-	0.1	1.8	0.5	62.9	0.3	9.8	0.8	-	1.1	-	0.5	12.4
02C	0.4	0.1	0.2	1.8	1.7	-	1.8	11.0	0.8	16.5	1.1	-	1.0	5.0
03C	0.4	-	0.1	1.8	1.6	-	1.1	-	0.8	-	1.1	17.6	0.8	3.2
04C	0.8	-	0.2	2.0	1.7	-	3.2	2.1	0.8	-	1.1	-	1.3	0.7
06C	-	100.0	0.1	2.3	1.7	1.2	1.4	3.5	0.9	1.3	1.1	13.6	0.8	20.3
AVER	0.3	14.3	0.2	2.8	2.0	9.1	1.4	3.8	1.1	3.5	1.1	4.4	1.0	6.0
LESS	02C					02B		02B 02C		02C		03C 06C		02B,02C 06C
	0.0					0.2		1.1		0.2		0.0		1.1

TABLE II.4.1

Communications (degraded performance >20/outages >200)
Figures in per cent of total time. Month four or five weeks, as indicated.
(4 Oct 82 - 3 Apr 83)

Week/ Year	Subarray/per cent outage						
	01A	01B	02B	02C	03C	04C	06C
40/83	-	-	-	-	-	-	100.0
41	-	-	-	-	0.3	-	100.0
42	-	-	-	0.6	-	-	100.0
43	-	-	-	-	-	-	100.0
44	-	-	-	-	-	0.9	1.2
45	-	-	-	-	-	-	0.6
46	7.1	7.1	7.1	7.1	7.1	7.1	6.5
47	0.1	0.1	0.1	0.1	0.1	0.1	0.1
48	-	-	14.3	-	-	-	6.1
49	-	-	-	-	-	-	-
50	-	-	100.0	-	-	-	-
51	-	-	100.0	-	-	-	-
52	-	-	100.0	-	-	-	-
1/83	-	-	39.3	-	-	-	-
2	-	-	-	-	-	-	7.1
3	-	-	-	4.7	-	8.4	7.1
4	-	-	-	42.8	-	-	-
5	-	-	-	66.1	-	-	-
6	-	-	-	-	-	-	-
7	-	-	-	-	-	-	5.3
8	-	-	-	-	-	-	-
9	-	-	-	-	24.4	-	0.1
10	0.4	0.4	0.4	0.4	63.7	0.4	9.2
11	-	-	-	-	-	-	26.9
12	-	-	-	-	-	-	14.3
13	-	-	-	-	-	-	17,8

TABLE II.4.2

III. IMPROVEMENTS AND MODIFICATIONS

III.1 NORSAR on-line system using IBM 4331/4341 and MODCOMP Classic

We refer to the detection processor operation statistics for detailed performance of the new system.

During this reporting period we finished array monitor control (AMC) programs. We have converted the programs and operational routines that were used for the old SPS-system. However, the system has now capabilities for monitoring that were not easily accessible using the 360 system. Using the graphic displays we may now do extensive visual control of the test period, that is, we may for instance inspect the individual broadband pulses and sine wave calibration patterns to verify the quality of the instruments.

The IBM 2701 synchronous controller which interfaces IBM 4331 with the MODCOMP system had one serious breakdown. It was only due to our own skilled technician that the system was brought up in satisfactory status again. In fact, this unit has been functioning with even fewer bit-errors during data transfer after this breakdown. Data checks (bit-errors) on this unit are now rarely observed.

We have, however, had occasional data losses due to the sharing of disk between the IBM 4331 and 4341. Data from the array are written on disk by 4331 and are read from the same disk by 4341. The IBM 3370 disk drives are organized in so-called strings. On one string we had disks containing data from the on-line system and disks containing normal user area and system disks. Since the 4341 computer is significantly faster than the 4331 computer, this system did occasionally block the slower machine from getting access to the disk. The follow-on result of this was that the disk recording on 4331 was going slower than the data was coming in. This could in periods cause loss of up to a minute of data. We solved this problem by doing two things: first, we reorganized disk strings to separate data disks from system disks; second, we reorganized programs on 4341 to read more data per read accesss. Using 4341 and 3370 disks,

a single read operation will always have 30 Msec search plus data transfer. Reading 0.5 sec of data will hold the disk for 33.4 Msec, whereas reading 12.0 sec of data will hold the disk for 63 Msec, i.e., by doubling the time we keep the disk busy, we may get 24 times more data to work with.

The result of these operations is that the 4341 uses the shared disk significantly fewer times per time unit. By applying this method to all programs we have succeeded in completely removing this form for loss of data.

During the second half of this reporting period we also started using the shared disk principle for the programs, that is, the programs running on the 4331 computer are loaded from shared disk. We therefore now do all program development/changes on the 4341 system, and a new version is set out in operation, causing less than 2 minutes drop in data recording.

On the MODCOMP system we have experienced that the 7th line may after a few days of continuous operation loose synchronization. We may correct this by commanding the MODCOMP to resynchronize the line (by in fact doing this on the 4341 system, which signals 4331 to send the command to MODCOMP), or restart the MODCOMP system. A complete restart of the MODCOMP causes less than one minute data drop. We have therefore preferred to restart the MODCOMP system up to twice a week to insure complete resynchronization of all lines and correct timing. This effect is a result of the SLEM communication being critically time dependent. The newer (compared to SPS) communication interfaces do handle some telephone line problems better, causing less number of transmission errors, but these corrections need time and the system as a whole may have problems in keeping all seven lines exactly synchronized. We have verified this by dropping subarray beamforming and filtering to see whether the high load on the system could be the problem, however, this does not seem to be a problem. In conclusion, we do not see any data-loss problem here, since the restart or resynchronization twice a week will secure the overall performance of the system.

The implementation of an IBM Series 1 front-end processor has given the opportunity to dial the NORSAR computer center from a remote location. Using a cheap, standard ASCII-type terminal, we may dial the center and use the facilities of the 4341 system. This has been used by DP operators to check the status of the system. In fact, we have verified that this may also be done from Washington, D.C., or any other place, using special 300 baud modems.

Improvements of the system now would be to exchange the 2701 communication controller with a direct IBM channel interface device on the MODCOMP. The main reason is to avoid having a device that is 20 years old, and which in the near future no longer will be supported by IBM. (However, NORSAR is glad to have a technician who is able to repair components on such devices.) Another gain we would experience by doing so is that the data transfer time between IBM and MODCOMP will be reduced by a factor of 5, which will free some of the load in both ends.

The next improvement step would be to build up backup systems. Today we may run the IBM part of the system on either 4331 or 4341, but there is no backup for MODCOMP. There are several ways to do this: One is of course to have an identical MODCOMP system as backup. Another is to move subarray beamforming and filtering over to the IBM side (if capacity). This reduces the requirements for the MODCOMP backup machine, and increases the possibilities for testing new DP processors on the IBM side. This latter way reduces the MODCOMP system to a pure communication path to the subarrays. This is important since the next step in future improvements of the NORSAR array would be on the instrument side, that is, the SLEM itself might be considered replaced.

J. Fyen
T. Hoff
R. Paulsen

Appendix to III.1 - Program examples, corrections to NORSAR Scientific Report No. 1-82/83

The following are parts of a FORTRAN G1 program that can extract data from NORSAR high-rate data block.

```
      LOGICAL*1 NRDATA(1372)                                                ONLOO740
      LOGICAL*1 NRID(2),NRTIME(4),NRGEN(2),AUTSA(2),AUTSEI(21)              CNLOO75O
      LOGICAL*1 MANSA(2),MANSEI(21),MULTI(7),PAD,LOGR1(262),LOGR2(262)      ONLOO760
      LOGICAL*1 LOGR3(262),LOGR4(262),LOGR5(262),LOGR(1310)                 ONLOO770
C                                                                           ONLOO780
      EQUIVALENCE (NRDATA,NRID),(NRDATA(3),NRTIME),(NRDATA(7),NRGEN),       CNLOO81O
     *(NRDATA(9),AUTSA),(NRDATA(11),AUTSEI),(NRDATA(32),MANSA),             ONLOO82O
     *(NRDATA(34),MANSEI),(NRDATA(55),MULTI),(NRDATA(62),PAD),              ONLOO83O
     *(NRDATA(63),LOGR1,LOGR),(NRDATA(325),LOGR2),(NRDATA(587),LOGR3),      CNLOO84O
     *(NRDATA(849),LOGR4),(NRDATA(1111),LOGR5)                              CNLOO85O
C                                                                           ONLOO86O
      LOGICAL*1 LOGREC(262),STATUS(10),SDBL(18,2,7)                         ONLOO87O
      INTEGER*2 SDB(9,2,7)                                                  ONLOO88O
      EQUIVALENCE(LOGREC,STATUS),(LOGREC(11),SDBL,SDB)                      CNLOO89O
C

  .......

C
      READ THE EQUIVALENT OF 0.5 SECONDS DATA  (1372 BYTES NRDATA)
C
C   PICK UP SINGLE SENSORS, SP FROM NORSAR ARRAY                            ONLO2000
C                                                                           ONLO2010
C   N2040 = 1 FOR 10 HZ                                                     ONLO2020
C   N2040 = 2 FOR 20 HZ                                                     ONLO2020
C                                                                           ONLO2030
      DO 3000 ILOG=1,5                                                      ONLO2040
C                                                                           ONLO205O
      ILDISP =(ILOG-1)*262                                                  ONLO2060
C                                                                           ONLO2080
      DO 2100 I=1,262                                                       ONLO2090
 2100 LOGREC(I) = LOGR(I+ILDISP)                                            ONLO210O
C                                                                           ONLO2110
      DO 2400 I20=1,N2040                                                   ONLO2120
C                                                                           ONLO213O
C                                                                           ONLO214O
      DO 2400 ISUB=   1,  7                                                 ONLO2170
C                                                                           ONLO2180
      ICWODW = SDB(1,I20,ISUB)                                              ONLO219O
C                                                                           ONLO22OO
C     IF( ICWODW .NE. 32 ) GO TO ERRGR                                      ONLO2210
C                                                                           ONLO2230
      DO 2320 ISNS=     1,    6                                             ONLO224O
C                                                                           ONLO225O
      ISAMP = ISAMP+1                                                       ONLO226O
      SAMP(ISAMP) = SDB(3+ISNS,I20,ISUB)/4                                  ONLO2270
C                                                                           ONLO2280
C                                                                           ONLO2300
 2320 CONTINUE                                                              ONLO2310
C                                                                           ONLO2320
C                                                                           ONLO2340
 2400 CONTINUE                                                              ONLO235O
C                                                                           ONLO2360
C                                                                           ONLO2480
 3000 CONTINUE                                                              ONLO249O
C                                                                           ONLO2500

  ......

C                                                                           CNLO2640
C   LOW RATE SENSOR DATA EXTRACTION                                         ONLO2640
C   SEE NORSAR SCIENTIFI REPORT NO. 1-82/83                                 ONLO2640
C                                                                           ONLO2650
```

III.2 Description of NORSAR recording system

Over the last few years, the number of independent recording system used at NORSAR has increased steadingly, and with that the need for easy and standardized retrieval of information about response characteristics and quantification levels. This has now been done in the form of a subroutine from which the desired information is returned following the entering of system number and frequency. The call is as follows:

```
CALL SPSYST (J, FREQ, RESP, GAIN, SENS, CODE, NSYS, IERR)
```

where input is

J = System number
FREQ = Frequency (Hz) for which response values are wanted

and output is

RESP = Response value relative to 1 Hz
GAIN = Response in NM/QU at 1 Hz for digital systems
SENS = Absolute magnification at 1 Hz for analog systems
CODE = System name (REAL * 8)
NSYS = Number of system responses on file
IERR = Error code, 0 = ok, 1 otherwise

The data base consists presently of 19 systems as described in Table III.2.1, where much relevant information is given, except for specifications about amplifiers and AD-convertors. Only two of the systems (5-6) are analog, based on MEQ-800 recorders. It should be emphasized that phase information is not given for any of the systems.

SYSTEM NO.	TYPE	RECORDING UNIT(S)	PREAMPL. (DB)	SEISM. TYPE	FILTER (HZ)	FILTER (DB/OCT)	QUANT. (NM/QU)	COMMENTS
1	NORSAR	MODCOMP/IBM	72	HS-10	4.75	24	0.0427	STANDARD NORSAR RECORDING AT NDPC
2	NORSAR	MODCOMP/IBM	72	HS-10	8.0	24	0.0427	STANDARD NORSAR RECORDING AT NDPC
3	SNSN	PDP 11/34	80	S-13	12.5	18	0.189	SOUTHERN NORWAY SEISMIC NETWORK (ANALOG TO NDPC)
4	SGSN	DDS-1105	72	SS-1	12.5	12	0.854	STIEGLER'S GORGE SEISMIC NETWORK (TANZANIA)
5	FIELD SYSTEM	MEQ-800	78	L-4C	-		-	ANALOG FIELD RECORDING , MAGNIFICATION 24547
6	FIELD SYSTEM	MEQ-800	78	L-4C	10.0		-	ANALOG FIELD RECORDING , MAGNIFICATION 22909
7	FIELD SYSTEM	DR-100	66	S-6000	-		14.286	DIGITAL FIELD RECORDING
8	FIELD SYSTEM	DR-100	66	S-6000	10.0		13.333	DIGITAL FIELD RECORDING
9	NORESS (06C)	MODCOMP/IBM	72	HS-10	12.5	18	0.3416	ANALOG TRANSMISSION TO MODCOMP AT NDPC
10	FIELD SYSTEM	PDR-2	60+42	S-13	25.0	12	0.0738	DIGITAL FIELD RECORDING
11	SNSN	PDR-2	80+42	S-13	25.0	18	0.000738	RECORDING OF SNSN DATA AT NDPC
12	NORSAR SUB.	PDR-2	72+42	HS-10	25.0	12	0.000334	RECORDING OF NORSAR DATA IN SUBARRAY CENTERS
13	NORESS (06C)	MODCOMP/IBM	82	SS-1	12.5	18	0.355	ANALOG TRANSMISSION FROM 06C TO MODCOMP AT NDPC
14	NORSAR (02B)	MODCOMP/IBM	78	S-500	12.5	18	0.320	ANALOG TRANSMISSION FROM 02B TO MODCOMP AT NDPC
15	NORSAR	SPS/IBM	72	S-500	8.0	24	0.0968	STANDARD NORSAR EXCEPT FOR SEISMOMETER
16	NORSAR SUB.	PDR-2	72+42	HS-10	50.0	12	0.000334	RECORDING OF NORSAR DATA IN SUBARRAY CENTERS
17	NORSAR SUB.	PDR-2	72+42	HS-10	12.5	12	0.000334	RECORDING OF NORSAR DATA IN SUBARRAY CENTERS
18	NORESS (06C)	PDR-2	82+42	SS-1	50.0	12	0.00100	RECORDING OF NORESS DATA AT 06C
19	NORESS (06C)	PDR-2	82+42	SS-1	12.5	12	0.00100	RECORDING OF NORESS DATA AT 06C

Table III.2.1 Description of the 19 recording systems used at NORSAR over the last few years, with recording unit, amplification, seismometer type, anti-aliasing filter, quantification at 1 Hz, and comments.

The standard NORSAR system (1,2,15) is gain-ranged in the following way:

Quantum levels	Steps	NM/QU
1-127	1	0.0427
128-511	4	0.1708
512-2047	16	0.6832
2048-8191	64	2.7328

The other system with gain-ranging is the Kinemetrics PDR-2, where there is a 12 bit mantissa (±2047 QU) and a 3 bit Log (base 2) gain value with 7 steps from 2^0 (0 dB) for the strongest signals to $2^7 = 128$ (42 dB) for the weakest signals. The gain switching logic is such that the system is slow to amplify but fast to attenuate.

The relative response values for different frequencies for all the systems are given in Table III.2.2, with 3 values per octave in frequency. These are the values that are on file (in SPSYST), and values for other frequencies are obtained by linear interpolation between the two closest points.

The relative response functions are plotted in Fig. III.2.1 for all of the systems and in Fig. III.2.2 for the systems that have been used more frequently lately. The curves are mostly based on theoretical values, although most of them are also checked by independent calibration. It should be emphasized that the wide frequency range has been chosen for reasons of convenience, values on the flanks have been extrapolated and are therefore not necessarily realistic.

Weather stations (wind direction and speed)

Two weather stations have recently been installed at NORSAR, one at NORESS (06C) and one at subarray 01A.

SYSTEM FREQ	1	2	3	4	5	6	7	8	9	10	11	12	13	14	15	16	17	18	19
0.10	2.85	2.85	2.85	2.85	3.32	3.32	3.80	3.80	2.85	2.85	2.85	2.85	2.85	3.32	3.32	2.85	2.85	2.85	2.85
0.13	2.55	2.55	2.55	2.55	2.98	2.98	3.42	3.42	2.55	2.55	2.55	2.55	2.55	2.98	2.98	2.55	2.55	2.55	2.55
0.16	2.25	2.25	2.25	2.25	2.64	2.64	3.04	3.04	2.25	2.25	2.25	2.25	2.25	2.64	2.64	2.25	2.25	2.25	2.25
0.20	1.95	1.95	1.95	1.95	2.30	2.30	2.66	2.66	1.95	1.95	1.95	1.95	1.95	2.30	2.30	1.95	1.95	1.95	1.95
0.25	1.65	1.65	1.65	1.65	1.96	1.96	2.28	2.28	1.65	1.65	1.65	1.65	1.65	1.96	1.96	1.65	1.65	1.65	1.65
0.32	1.35	1.35	1.35	1.35	1.62	1.62	1.90	1.90	1.35	1.35	1.35	1.35	1.35	1.62	1.62	1.35	1.35	1.35	1.35
0.40	1.05	1.05	1.05	1.05	1.28	1.28	1.52	1.52	1.05	1.05	1.05	1.05	1.05	1.28	1.28	1.05	1.05	1.05	1.05
0.50	0.75	0.75	0.75	0.75	0.94	0.94	1.14	1.14	0.75	0.75	0.75	0.75	0.75	0.94	0.94	0.75	0.75	0.75	0.75
0.63	0.47	0.47	0.47	0.47	0.60	0.60	0.76	0.76	0.47	0.47	0.47	0.47	0.47	0.60	0.60	0.47	0.47	0.47	0.47
0.79	0.22	0.22	0.22	0.22	0.25	0.25	0.38	0.38	0.22	0.22	0.22	0.22	0.22	0.25	0.25	0.22	0.22	0.22	0.22
1.00	0.0	0.0	0.0	0.0	0.0	0.0	0.0	0.0	0.0	0.0	0.0	0.0	0.0	0.0	0.0	0.0	0.0	0.0	0.0
1.26	-0.18	-0.18	-0.18	-0.18	-0.17	-0.16	-0.35	-0.35	-0.18	-0.18	-0.18	-0.18	-0.18	-0.18	-0.18	-0.18	-0.18	-0.18	-0.18
1.58	-0.33	-0.33	-0.33	-0.33	-0.29	-0.27	-0.65	-0.65	-0.33	-0.33	-0.33	-0.33	-0.33	-0.34	-0.34	-0.33	-0.33	-0.33	-0.33
2.00	-0.45	-0.45	-0.45	-0.45	-0.37	-0.34	-0.86	-0.86	-0.45	-0.45	-0.45	-0.45	-0.45	-0.48	-0.48	-0.45	-0.45	-0.45	-0.45
2.51	-0.55	-0.55	-0.55	-0.55	-0.45	-0.41	-1.00	-0.97	-0.55	-0.55	-0.55	-0.55	-0.55	-0.60	-0.60	-0.55	-0.55	-0.55	-0.55
3.16	-0.65	-0.65	-0.65	-0.65	-0.53	-0.48	-1.10	-1.05	-0.65	-0.65	-0.65	-0.65	-0.65	-0.70	-0.70	-0.65	-0.65	-0.65	-0.65
3.98	-0.68	-0.75	-0.75	-0.75	-0.62	-0.56	-1.20	-1.14	-0.75	-0.75	-0.75	-0.75	-0.75	-0.80	-0.80	-0.75	-0.75	-0.75	-0.75
5.01	-0.50	-0.85	-0.85	-0.85	-0.72	-0.64	-1.30	-1.22	-0.85	-0.85	-0.85	-0.85	-0.85	-0.90	-0.90	-0.85	-0.85	-0.85	-0.85
6.31	-0.20	-0.93	-0.95	-0.93	-0.81	-0.69	-1.40	-1.28	-0.95	-0.95	-0.95	-0.95	-0.95	-1.00	-0.98	-0.95	-0.95	-0.95	-0.95
7.94	0.10	-0.90	-1.05	-0.98	-0.91	-0.73	-1.50	-1.32	-1.05	-1.05	-1.05	-1.05	-1.05	-1.10	-0.95	-1.05	-1.05	-1.05	-1.05
10.00	0.40	-0.60	-1.13	-1.00	-1.00	-0.73	-1.60	-1.33	-1.13	-1.15	-1.15	-1.15	-1.13	-1.18	-0.65	-1.15	-1.13	-1.15	-1.15
12.59	0.70	-0.30	-1.10	-0.98	-1.10	-0.71	-1.70	-1.31	-1.10	-1.25	-1.25	-1.25	-1.10	-1.15	-0.35	-1.25	-1.06	-1.25	-1.25
15.85	1.00	-0.00	-0.90	-0.93	-1.20	-0.67	-1.80	-1.28	-0.90	-1.35	-1.35	-1.35	-0.90	-0.95	-0.05	-1.35	-0.96	-1.35	-1.35
19.95	1.30	0.30	-0.70	-0.85	-1.30	-0.63	-1.90	-1.23	-0.70	-1.43	-1.43	-1.43	-0.70	-0.75	0.25	-1.45	-0.86	-1.45	-1.43
25.12	1.60	0.60	-0.50	-0.75	-1.40	-0.58	-2.00	-1.18	-0.50	-1.36	-1.35	-1.36	-0.50	-0.55	0.55	-1.55	-0.76	-1.55	-1.36
31.62	1.90	0.90	-0.30	-0.65	-1.50	-0.53	-2.10	-1.13	-0.30	-1.26	-1.15	-1.26	-0.30	-0.35	0.85	-1.65	-0.66	-1.65	-1.26
39.81	2.20	1.20	-0.10	-0.55	-1.60	-0.47	-2.20	-1.08	-0.10	-1.16	-0.95	-1.16	-0.10	-0.15	1.15	-1.73	-0.56	-1.73	-1.16
50.12	2.50	1.50	0.10	-0.45	-1.70	-0.42	-2.30	-1.03	0.10	-1.06	-0.60	-1.06	0.10	0.05	1.45	-1.66	-0.46	-1.66	-1.06
63.10	2.80	1.80	0.30	-0.35	-1.80	-0.37	-2.40	-0.98	0.30	-0.96	-0.20	-0.96	0.30	0.25	1.75	-1.56	-0.36	-1.56	-0.96
79.43	3.10	2.10	0.50	-0.25	-1.90	-0.33	-2.50	-0.93	0.50	-0.86	0.20	-0.86	0.50	0.45	2.05	-1.46	-0.26	-1.46	-0.86
100.00	3.40	2.40	0.70	-0.15	-2.00	-0.28	-2.60	-0.88	0.70	-0.76	0.60	-0.76	0.70	0.65	2.35	-1.36	-0.16	-1.36	-0.76

Table III.2.2 Systems response values for the 19 systems described in Table III.2.1. The values are logarithmic, and correspond to the curves plotted in Figs. III.2.1-2.

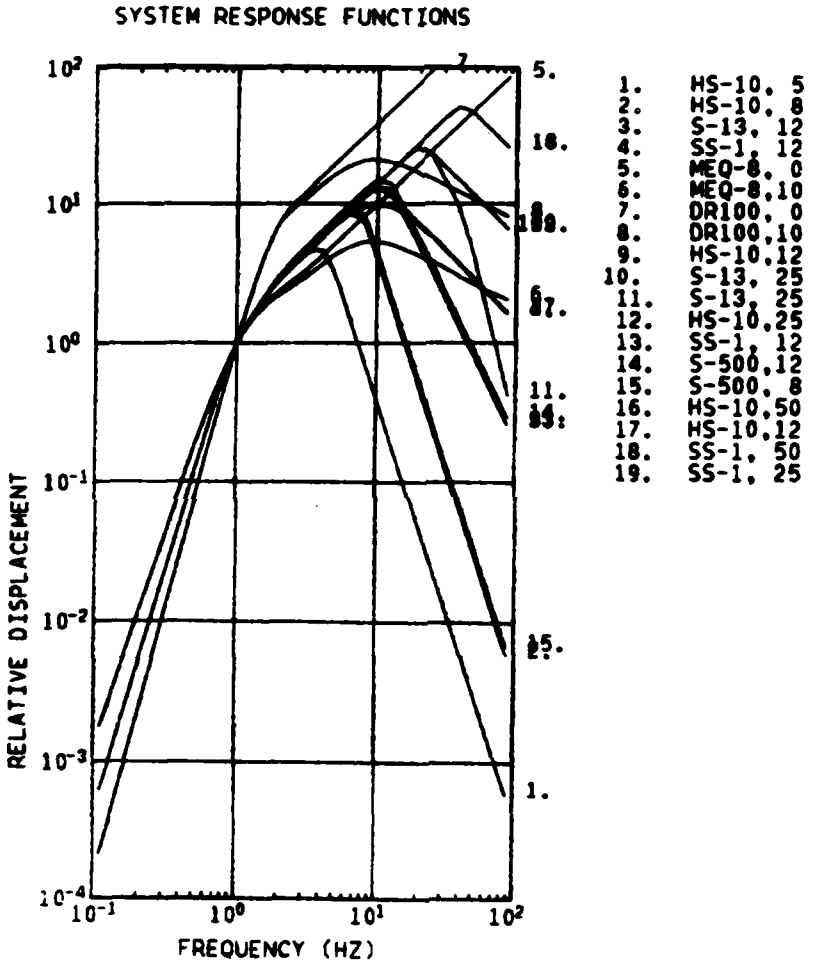

Fig. III.2.1 System response for all 19 systems described in this section. The system numbers refer to the numbers in Tables III.2.1-2.

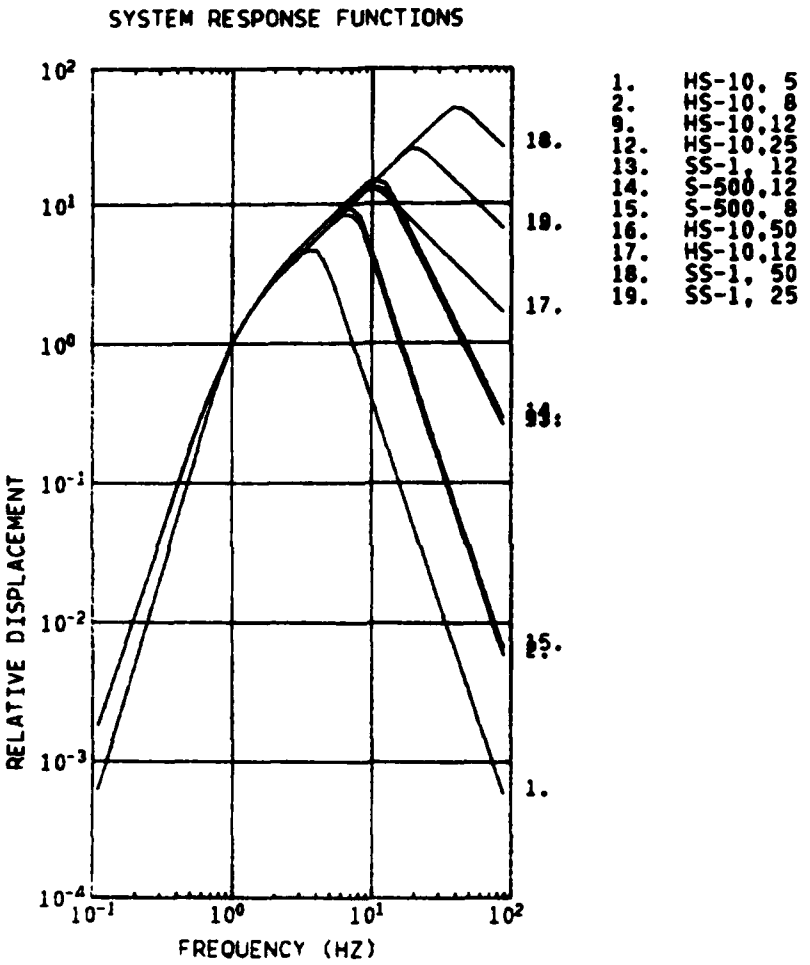

Fig. III.2.2 System response for the systems more recently used in the analysis of NORSAR and NORESS data. The system numbers refer to the numbers in Tables III.2.1-2.

The wind data from NORESS are transmitted in analog form to the Modcomp at NDPC (system 13 in Table III.2.1), with wind direction in channel 7 and wind speed in channel 8. At subarray 01A, equivalent data are recorded at channels 01A05 and 01A03, respectively. The channels are calibrated as follows:

Channel	Data	5V level	mV/QU	Quantification
NORESS 7	Direction	540°	3.40	0.367 deg/QU
NORESS 8	Speed	50 m/s	3.40	0.034 m/s/QU
01A05	Direction	540°	0.61	0.066 deg/QU
01A03	Speed	50 m/s	0.61	0.0061 m/s/QU

Note here that the wind speed increases linearly from 0 to 50 m/s corresponding to 0 to 5 volts in output, while the same output range for the wind direction corresponds to a linear clockwise increase from 0° (north) to 540° (south). A further increase will cause the output to drop from 5 volts = 540° to 5/3 volts = 180°, while a counter-clockwise change around 0° will cause the output to increase from 0 volts = 0° to 10/3 volts = 360°. This is done, obviously enough, in order to reduce the number of sudden changes in the output level as the wind direction fluctuates around north or south.

H. Bungum

IV. FIELD INSTRUMENTATION AND MAINTENANCE ACTIVITIES

Improvements and modifications

Reference is made to Table IV.1 and IV.2 indicating the status of the SP instruments (original array), the modified NORESS array, and the expanded 02B subarray (telemetry stations), which are all unchanged compared to status in the previous report.

The expanded 02B subarray was fully operational 5 November 1982.

Fig. IV.1 shows the expanded 02B array, and Table IV.3 gives the coordinates for the stations.

The 06C NORESS array is shown in Fig. IV.2.

Preparatory work in connection with the planned expansion of the NORESS array continued at the maintenance center (NMC) in March.

In connection with a noise study program, recording of noise data started early in January and continued throughout the reporting period, reference Table IV.4.

Subarray Normally	Instr. No. within SA	Ch. No. on NORSAR Data Tape	Time of change 10/08/82	10/28/82	10/29/82
01A	1	1	-	-	8 Hz filter
(1)	2	2	1)	-	8 Hz filter
	3	3	-	2)	-
	4	4	-	-	-
	5	5	-	3)	-
	6	6	-	-	Normal
01B	1	7	-	-	-
(2)	2	8	-	-	-
	3	9	-	-	-
	4	10	-	-	-
	5	11	-	-	-
	6	12	-	-	-
02B	1	13	-	-	-
(3)	2	14	-	-	-
	3	15	-	-	-
	4	16	-	-	-
	5	17	-	-	-
	6	18	-	-	-
02C	1	19	-	-	-
(4)	2	20	-	-	-
	3	21	-	-	-
	4	22	-	-	-
	5	23	-	-	-
	6	24	-	-	-

1) Data from borehole at site 1 (60 m hole) to SP ch 02 (in CTV)
2) Wind speed to SP ch 03 (in CTV)
3) Wind direction to SP ch 05 (in CTV)

TABLE IV.1

Status of NORSAR SP instruments recorded on data tape.
(Page 1)

Subarray Normally	Instr. No. within SA	Ch. No. on NORSAR Data Tape	Time of Change		
			10/08/82	10/28/82	10/29/82
03C	1	25	-	-	-
(5)	2	26	-	-	-
	3	27	-	-	-
	4	28	-	-	-
	5	29	-	-	-
	6	30	-	-	-
04C	1	31	-	-	-
(6)	2	32	-	-	-
	3	33	-	-	-
	4	34	-	-	-
	5	35	-	-	-
	6	36	-	-	-
06C	1	37	-	NORESS station no. 1 (Fig. IV.2)	-
(7)	2	38	-	-"- 3	-
	3	39	-	-"- 8	-
	4	40	-	-"- 9	-
	5	41	-	-"- 10	-
	6	42	-	-"- 11	-

TABLE IV.1
(Page 2)

Subarray Normally	NORSAR Analog ch. at NDPC	Time of Change 10/30/81	10/04/82	10/21/82
06C (NORESS)	1	NORESS station nr. 1 *	-	NORESS sta. no. 2, VERT seis SS-1
	2	- " - 3	-	- " - NS seis SS-1
	3	- " - 4	-	- " - EW seis SS-1
	4	- " - 5	NORESS sta. no. 6, VERT seis SS-1	-
	5	- " - 7	- " - NS seis SS-1	-
	6	- " - 6	- " - EW seis SS-1	-
	7	- " - 8	-	- " - Wind direction
	8	- " - 9	-	- " - Wind speed
	9			02B (telemetry) 1 S-500
	10			- " - 2 "
	11			- " - 3 "
	12			- " - 4 "
	13			- " - 5 "
	14			- " - 6 "
	15			
	16			
	17			
	18			

* (see Fig. IV.2)

TABLE IV.2

Status of NORESS and 02B (telemetry stations) and their connections to analog channels at NDPC (1-14)

Station No.	Latitude (N)	Longitude (E)
1	61.068344	11.156468
2	61.101196	11.161124
3	61.091309	11.166824
4	61.107315	11.174083
5	61.084824	11.174442
6	61.049728	11.158080

TABLE IV.3

Preliminary geographical coordinates
for the new 02B stations.

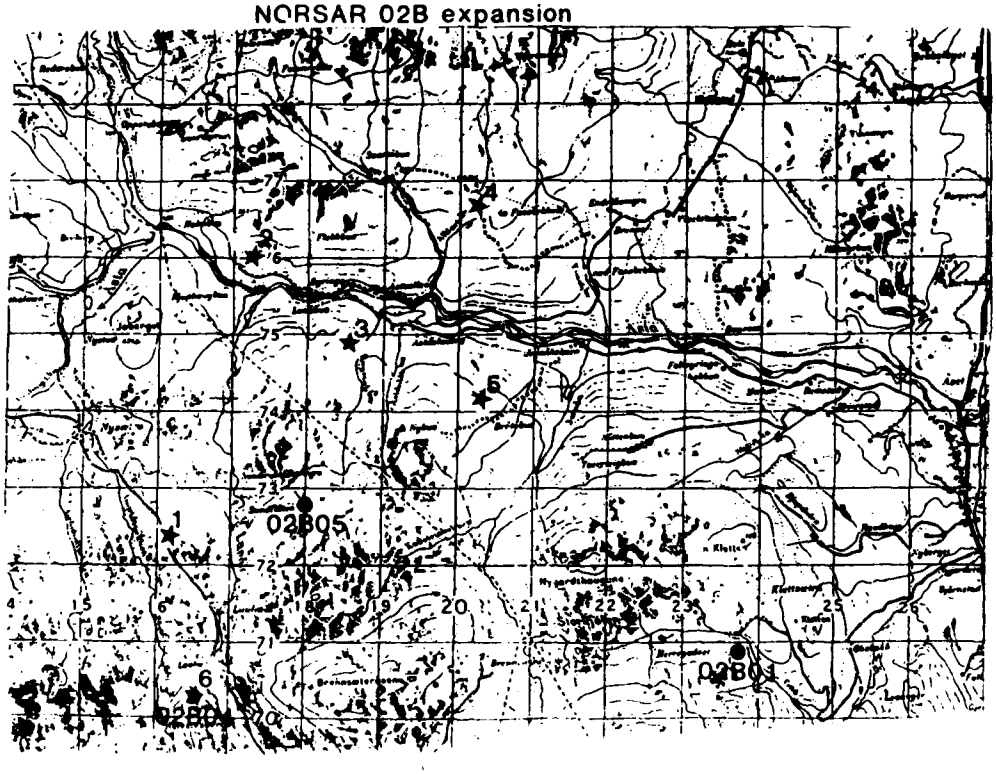

Fig. IV.1 The six new stations in the expanded 02B array.

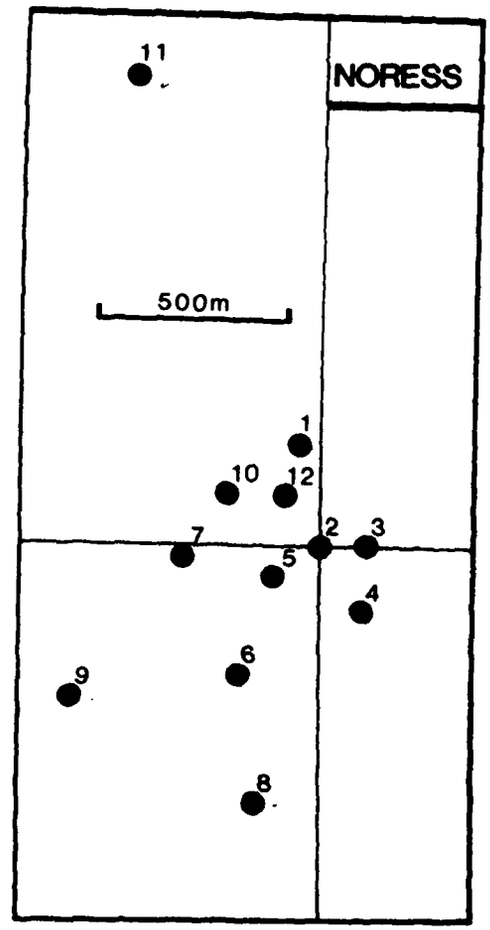

Fig. IV.2 Station numbering in the NORESS array.

Activities in the field and at the NORSAR Maintenance Center

This section outlines in brief the activities in the field and at the NORSAR Maintenance Center (Table IV.4). Table IV.5 indicates corrective/preventive maintenance in the field.

SA/Area	Task	Date
01A	Installation of a wind station	(Week .. Oct)
01A	SP seism. installed in borehole	(7,29 Oct)
06C, NORESS	Inst. of two sets of 3-comp SP seism. (SS-1) & a wind station	(1,4,5,6 Oct)
02B, telemetry sta.	Inst. of equipment at the new stations continued	(13,14,18,19, 20 Oct)
SNSN, Evje	Equipment repaired	(22,23 Oct)
02B, telemetry sta.	Inst. of equipment finished and fully operational	(5 Nov)
06C, NORESS	Attempts to locate new sites	(10,11 Nov)
02B	Subarray visited due to power outage	(20 Dec)
02B, telemetry sta.	Snow/ice problems reducing charging effect of solar cells	
06C, NORESS	Array expansion	(1,15,16 Dec)
NORSAR	Meeting at NORSAR, Sandia repres.	(6 Dec)
06C area	P.W. Larsen guided Sandia and NORSAR repres. in connection with new array	(8 Dec)
03C area	Assistance to Rena Power Co. in connection with power outage	(3,4 Jan)
03C area	Noise data recording	(11 Jan)
02B area	-"-	(12 Jan)
02C area	-"-	(19 Jan)
04C area	-"-	(25 Jan)
02B, telemetry sta.	Sta. 1,4 - battery replaced	(14,20 Jan)
02B area	Noise data recording	(1,25 Feb)
06C, CTV	T.O.D. generator hooked up for MODCOMP timing comparison	(7 Feb)
06C area	Noise data recording	(8,22 Feb)
06C area	Weather station checked	(9 Feb)
03C area	Localization of cable traces	(16,18 Feb)
01A area	Noise data recording	(24 Feb)
02B area	-"-	(1 Mar)
02B, telemetry sta.	Noise problem investigation cont.	(2 Mar)
01A area	Noise data recording	(3,28 Mar)
NMC	Activities mainly in connection with preparation of the planned expansion of the NORESS array	(4-23 Mar)
06C area	Noise data recording	(24,25 Mar)
NDPC	-"-	( )

TABLE IV.4

Period 1 Oct 82 - 31 Mar 83

Unit	SLEM Equipm.			SP Equipm.			LP Equipm.		
	Rep.	Adj.	Repl.	Rep.	Adj.	Repl.	Rep.	Adj.	Repl.
Seism. LP									
FP								1	
MP								1	
RCD, FP									3
RCD, MP									5
MP-bridge									1
Ampl. Ithaco									
LP									1
Ampl. RA-5									
SP						1			
Seism. SP									
Vert. (SS-1)									
NORESS					1				
SLEM									
Mux/ADC	1								

TABLE IV.5

Corrective/preventive maintenance work in the period.
1 Oct 82 - 31 Mar 83

Array status

As of 31 March 1983 the following channels deviated from tolerances:
01B01; 02B03,05; 02C06,08,09; 03C04; 04C01; 06C09.

01A 01 8 Hz filter
01A 02 -"- , 60 m borehole
01A 03 Wind speed measurements
01A 04 Attenuated 40 dB
01A 05 Wind direction measurements

O.A. Hansen

ABBREVIATIONS

CTV	-	Central Terminal Vault
EW	-	East-West
FP	-	Free period
LP	-	Long period
MP	-	Mass position
MUX	-	Multiplexer
NDPC	-	NORSAR Data Processing Center
NORESS	-	NORSAR Experimental Small-Aperture Subarray
NS	-	North-South
RCD	-	Remote centering device
SLEM	-	Seismic short and long period electronics module
SA	-	Subarray
SP	-	Short period

V. DOCUMENTATION DEVELOPED

Asudeh, I., 1982: P_n velocities beneath Iran, IPSL, 61, 136-142.

Bungum, H. and A.A. Nnko, 1983: Seismicity and tectonics of the Stiegler's Gorge area, Tanzania, Submitted for publication.

Doornbos, D.J., 1983: Observable effects of the seismic absorption band in the earth. Geophy. J. R. Astr. Soc., in press.

Tronrud, L.B., 1983: Semiannual Technical Summary, NORSAR Sci. Rep. No. 2-81/82, NTNF/NORSAR, Kjeller, Norway.

L.B. Tronrud

VI. SUMMARY OF TECHNICAL REPORTS/PAPERS PREPARED

VI.1 The absorption band effect on long-period body waves

It is generally appreciated that the effect of anelastic absorption on body wave amplitudes is most pronounced in the short-period band. However, in the presence of an absorption band in the mantle, the accompanying velocity dispersion is best observed in long-period body waves. This is because (1) dispersion represents an integral form of Q^{-1} in the band (in contrast to attenuation which represents a 'point property'), and (2) the mantle absorption band extends throughout the long-period range, but not throughout the short-period range of body waves. The last statement is an inference drawn by several authors in recent years, and it is confirmed in the present study. In this work the possibility is explored to use both the dispersion and the amplitude information in a procedure to separate absorption and source effects, and the procedure is applied to SRO/ASRO records of P waves from moderately sized deep focus events between 30 and 90°. The observations were compared to a synthetic purely elastic response, and the observed short-period onset was used to adjust the start time of the synthetic. The last procedure eliminates the effect of station residuals. The implicit assumption here is that the visible short-period onset is unaffected by the absorption; this can be justified later by the results of the analysis. The data are shown in Fig. VI.1.1; other information can be found in Doornbos (1983).

In all examples the long-period waveform is essentially delayed with respect to the synthetic, and the peak amplitude delay is used as an observational parameter. The delay must be explained as the combined effect of the source pulse and the anelastic dispersion. Since dispersion is relatively insensitive to details of an absorption model, we choose a convenient model: the relaxation model which is uniform in $\ln\tau$, within certain bounds τ_1, τ_2 (Liu, Kanamori and Anderson, 1976):

$$Q^{-1}(\omega) \sim 2 \operatorname{tg}^{-1} \left\{ \frac{\omega(\tau_2-\tau_1)}{1+\omega^2\tau_1\tau_2} \right\} \qquad (1)$$

Our measure of phase velocity dispersion is:

$$D(\omega) = c_\infty c(\omega) - 1 \simeq \overline{Q^{-1}(\omega)} \qquad (2)$$

where c_∞ and $c(\omega)$ are phase velocities at infinite frequency and at ω, and the overbar denotes the Hilbert transform. For the model (1):

$$D(\omega) \sim \ln(\tau_2/\tau_1) - \tfrac{1}{2} \ln\left(\frac{1+\omega^2\tau_2^2}{1+\omega^2\tau_1^2}\right) \qquad (3)$$

This model is convenient, since the resulting damping and dispersion become explicitly independent of the long-period cut-off τ_2, for $\omega\tau_2 \gg 1$. If also $\tau_2 \gg \tau_1$:

$$Q^{-1}(\omega) \simeq 2/\pi \; Q_m^{-1} \mathrm{tg}^{-1}(1/\omega\tau_1), \; D(\omega) \simeq \pi/2 \; Q_m^{-1} \ln(1+1/\omega^2\tau_1^2)$$

There is good evidence that $\omega\tau_2 \gg 1$ at body wave frequencies (Anderson and Given, 1982). The second condition $\tau_2 \gg \tau_1$ can be justified a posteriori. It sets the normalizing constant in equation (4) to π. In the present treatment we have further specified the model by assuming that Q_m^{-1} is given by PREM (which incorporates a long-period Q model). There is then one undetermined parameter τ_1.

In treating the source effect two approaches can be taken. The first is to ignore the effect, i.e., treat the source pulse as a delta function. It results in a maximum estimate for the cut-off frequency of the absorption band, i.e., an absolute minimum for τ_1. In the second approach we adopt a model for the source pulse and estimate the source and absorption parameters simultaneously. It is done by computing the RMS amplitude error, and the time residue, as a function of trial cut-off relaxation time τ_1.

The results of this experiment are shown in Fig. VI.1.2. The time residue and RMS error curve are consistent, and zero time residue corresponds to an absorption bandwidth near 0.2 Hz, i.e., τ_1 near 0.9 s. In the presence of noise and in the context of a single absorption band this constraint can be somewhat relaxed, and cut-off frequencies up to 1 Hz are admitted by the

data. The result represents the integrated effect of Q^{-1} along the wave path but it can be directly applied to correct body waves synthesized in purely elastic, or frequency independent Q, models. Since the present result is based on teleseismic records from deep events, it should be more representative of absorption in the lower mantle.

D.J. Doornbos

References

Anderson, D.L. and J.W. Given (1982): Absorption band Q model for the earth, J. Geophys. Res. 87, 3893-3904.

Doornbos, D.J. (1983): Observable effects of the seismic absorption band in the earth. Submitted for publication.

Liu, H.P., D.L. Anderson and H. Kanamori (1976): Velocity dispersion due to anelasticity: implications for seismology and mantle composition, Geophys. J.R. Astr. Soc. 47, 41-58.

Fig. VI.1.1 Observed short-period P wave (upper trace, record length 12 seconds), observed and synthetic long-period P wave (middle and lower trace, record length 60 seconds). The anelastic absorption effect is deleted from the synthetic, and note the time delay between the observed and synthetic waveform. Observations are numbered according to Doornbos (1983).

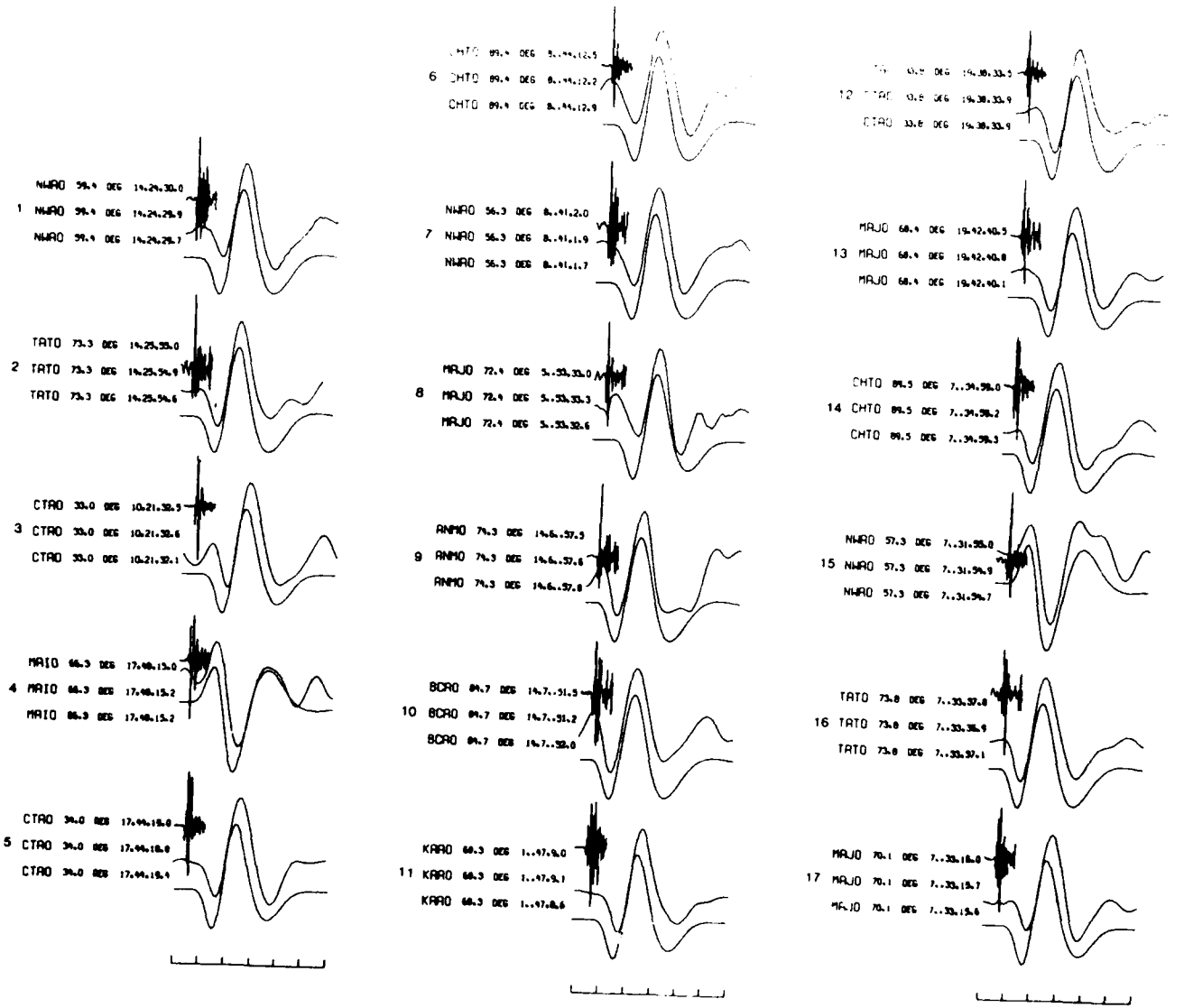
NWRO 59.4 DEG 14.24.30.0
1 NWRO 59.4 DEG 14.24.29.9
NWRO 59.4 DEG 14.24.29.7
TATO 73.3 DEG 14.25.35.0
2 TATO 73.3 DEG 14.25.34.9
TATO 73.3 DEG 14.25.34.8
CTRO 33.0 DEG 10.21.32.5
3 CTRO 33.0 DEG 10.21.32.6
CTRO 33.0 DEG 10.21.32.1
MRIO 66.3 DEG 17.48.15.0
4 MRIO 66.3 DEG 17.48.15.2
MRIO 66.3 DEG 17.48.15.2
CTRO 34.0 DEG 17.44.19.0
5 CTRO 34.0 DEG 17.44.18.8
CTRO 34.0 DEG 17.44.19.4
CHTO 89.4 DEG 8..44.12.5
6 CHTO 89.4 DEG 8..44.12.2
CHTO 89.4 DEG 8..44.12.9
NWRO 56.3 DEG 8..41.2.0
7 NWRO 56.3 DEG 8..41.1.9
NWRO 56.3 DEG 8..41.1.7
MRJO 72.4 DEG 5..53.33.0
8 MRJO 72.4 DEG 5..53.33.3
MRJO 72.4 DEG 5..53.32.6
ANMO 74.3 DEG 14.6..57.5
9 ANMO 74.3 DEG 14.6..57.6
ANMO 74.3 DEG 14.6..57.8
BCRO 84.7 DEG 14.7..51.5
10 BCRO 84.7 DEG 14.7..51.2
BCRO 84.7 DEG 14.7..52.0
KARO 68.3 DEG 1..47.9.0
11 KARO 68.3 DEG 1..47.9.1
KARO 68.3 DEG 1..47.8.6
12 DEG 19.38.33.5
DEG 19.38.33.9
33.6 DEG 19.38.33.9
MRJO 68.4 DEG 19.42.40.5
13 MRJO 68.4 DEG 19.42.40.8
MRJO 68.4 DEG 19.42.40.1
CHTO 89.5 DEG 7..34.58.0
14 CHTO 89.5 DEG 7..34.58.2
CHTO 89.5 DEG 7..34.58.3
NWRO 57.3 DEG 7..31.55.8
15 NWRO 57.3 DEG 7..31.54.9
NWRO 57.3 DEG 7..31.54.7
TATO 73.8 DEG 7..33.37.8
16 TATO 73.8 DEG 7..33.38.9
TATO 73.8 DEG 7..33.37.1
MRJO 70.1 DEG 7..33.18.8
17 MRJO 70.1 DEG 7..33.15.7
MRJO 70.1 DEG 7..33.15.6

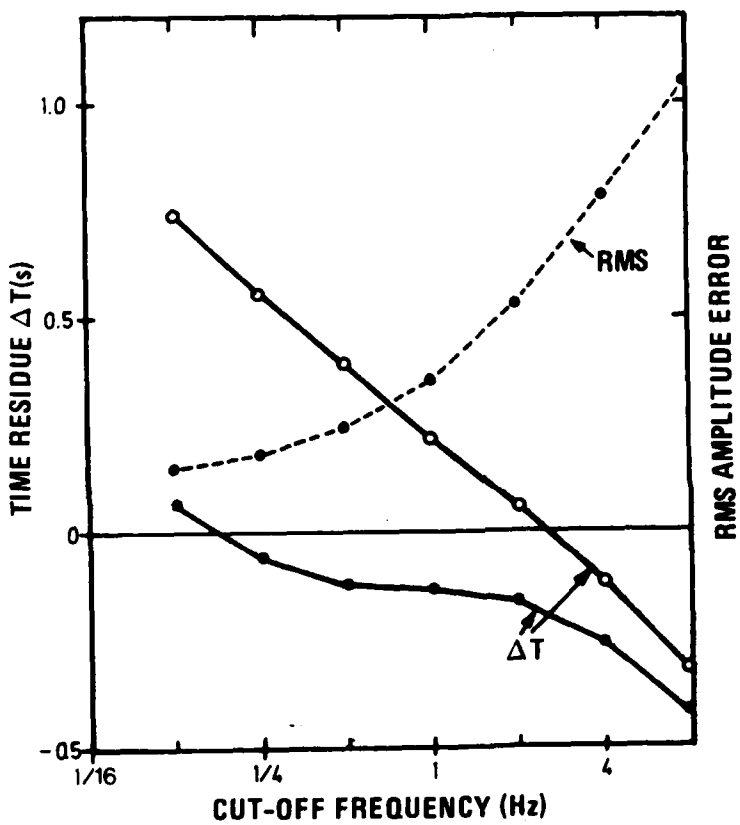

Fig. VI.1.2 Averaged time residue and RMS amplitude error in fitting a source and absorption model to the P wave data of Fig. VI.1.1, as a function of the high-frequency cut-off of the absorption band. The closed dots represent a solution with finite source effect. The open dots represent a solution where the source effect is ignored.

VI.2 The present seismic evidence for a boundary layer at the base of the mantle

The velocity structure at the base of the mantle has been the subject of a long-standing controversy. Velocity models proposed in the past encompass a range from positive to negative gradients; the three models shown in Fig. VI.2.1 are representative of different alternatives. This figure also shows two different interpretations of combined P and S velocity profiles, as a density effect or as a temperature effect. Note that models with velocities which are anomalous in the sense that the gradients with depth reverse and become negative, have recently been associated with a thermal boundary layer. In 1974, Cleary reviewed the available seismic evidence and concluded that a velocity reversal was likely. However, the data were interpreted mainly in a ray geometrical context and since diffraction effects can be significant, the evidence has been subject to criticism. Doornbos and Mondt (1979) applied diffraction theory to an extensive set of long-period P and SH data and still inferred a velocity reversal, although the thickness of the low-velocity zone was found to be much smaller than the 200 km conventionally assign to the D" layer. More recently, several authors find no evidence for a low-velocity zone (see, e.g., Ruff and Helmberger, 1982). In a recent contribution we have made use of new data from the SRO network and from the NORSAR array, in an attempt to reconcile the available evidence.

A typical example of long-period diffracted waves observed at the SRO network, is shown in Fig. VI.2.2. It is clear that the amplitude decay of SV in the core shadow zone is too strong to yield useful data, in agreement with a theoretical prediction for a range of possible models. Thus, only P and SH have been used here. Some striking examples of short-period diffracted P at the NORSAR array are given in Fig. VI.2.3. PKP from the same events are given for comparison, and the data to be used are based on an amplitude ratio of P and PKP at the periods 1 and 2 seconds. Altogether we have obtained long-period diffraction data from 16 events, long-period P from 25 events, and short-period P from 10 events.

In Figs. VI.2.4 and VI.2.5 the data are compared to calculated decay spectra and $dT/d\Delta$, using the models of Fig. VI.2.1. In the calculations, the extended WKBJ method (Langer's approximation) was applied to a piecewise smooth layered model. In this way the effect of both a velocity gradient and changes in the gradient are evaluated (Doornbos, 1981). The $dT/d\Delta$ curves of Fig. VI.2.4 reflect the fact that diffracted waves are usually dispersed. In analogy to phase and group velocity, we have introduced the phase and group slowness, $p(\omega)$ and $g(\omega)$, respectively. Their difference is

$$g(\omega) - p(\omega) = \omega \, dp/d\omega$$

and since this dispersion depends on the velocity gradient and its changes, it can be used as an additional diagnostic.

The observed low decay of long-period diffracted SH, the $dT/d\Delta$ values, and the apparent absence of dispersion, are all compatible with a relatively thin (< 100 km) low-velocity zone for S at the base of the mantle. The long-period SRO data lack the resolving power to settle the question for P. The results for short-period P as summarized in Fig. VI.2.5 strongly suggest that a comparable low-velocity zone for P exists, at least in the region sampled by the NORSAR data (beneath Central Asia). It is not inconsistent with a global average of short-period $dT/d\Delta$ and amplitude data near the core shadow boundary (also summarized in Fig. VI.2.5), but it should be mentioned that at least one recent study of short-period amplitudes gave results conflicting with the global average (Ruff and Helmberger, 1982). If this is to be 'explained' by lateral variations, then it should be added that the presence of lateral variations itself is not in conflict with boundary layer models. On balance, current thermal models appear to be consistent with (but not required by) the present seismic evidence.

D.J. Doornbos

References

Cleary, J.R. (1974): The D" region, Phys. Earth Planet. Int. 9, 13-27.

Doornbos, D.J. (1981): The effect of a second-order velocity discontinuity on elastic waves near their turning point, Geophys. J.R. Astr. Soc. 64, 499-511.

Doornbos, D.J. and J.C. Mondt (1979): P and S waves diffracted around the core and the velocity structure at the base of the mantle, Geophys. J.R. Astr. Soc. 57, 381-395.

Ruff, L.J. and D.V. Helmberger (1982): The structure of the lowermost mantle determined by short-period P-wave amplitudes, Geophys. J.R. Astr. Soc. 68, 95-119.

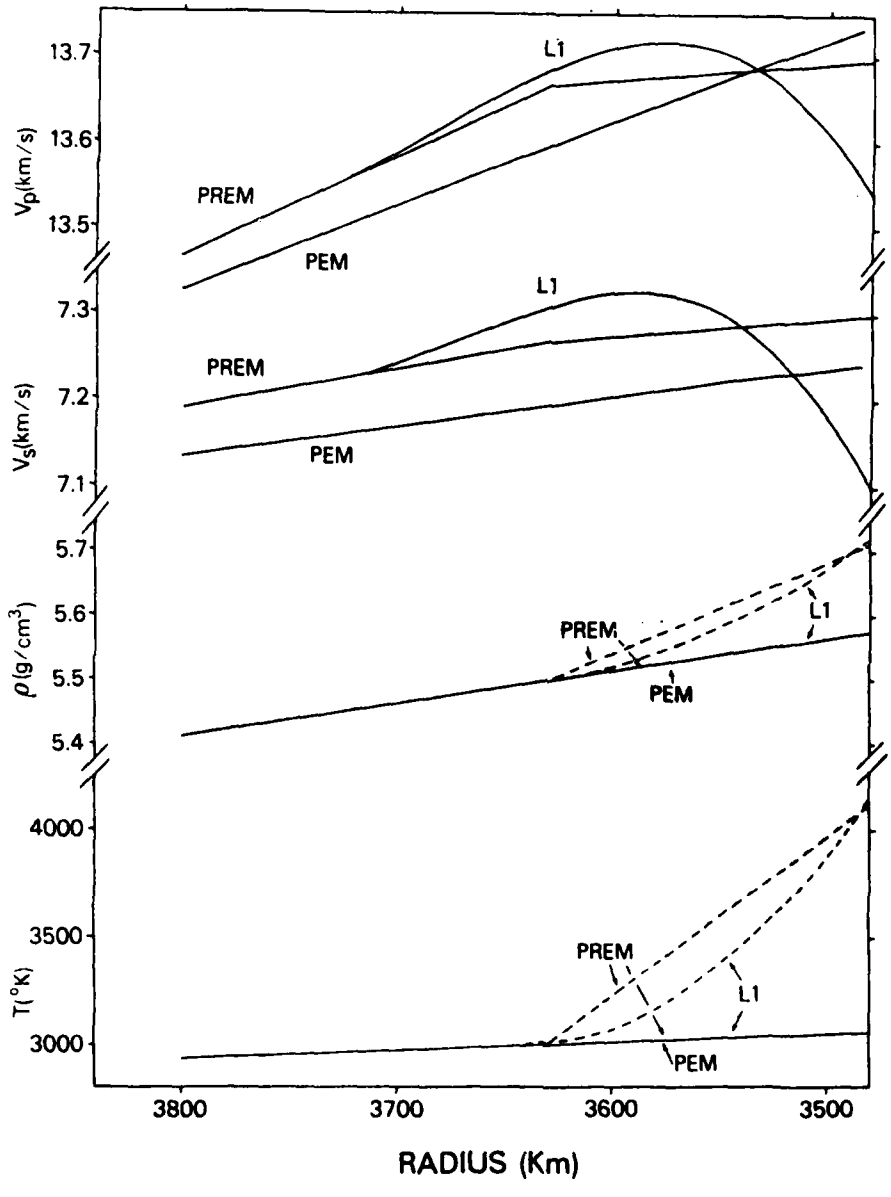

Fig. VI.2.1 Models of P and S velocity v_p, v_s, density ρ and temperature T in the lower mantle. The superdiabatic temperature profiles of PREM and L1 correspond to a homogeneous density (PEM profile), and the inhomogeneous density profiles correspond to the adiabatic temperature of PEM. Absolute temperatures have been arbitrarily fixed.

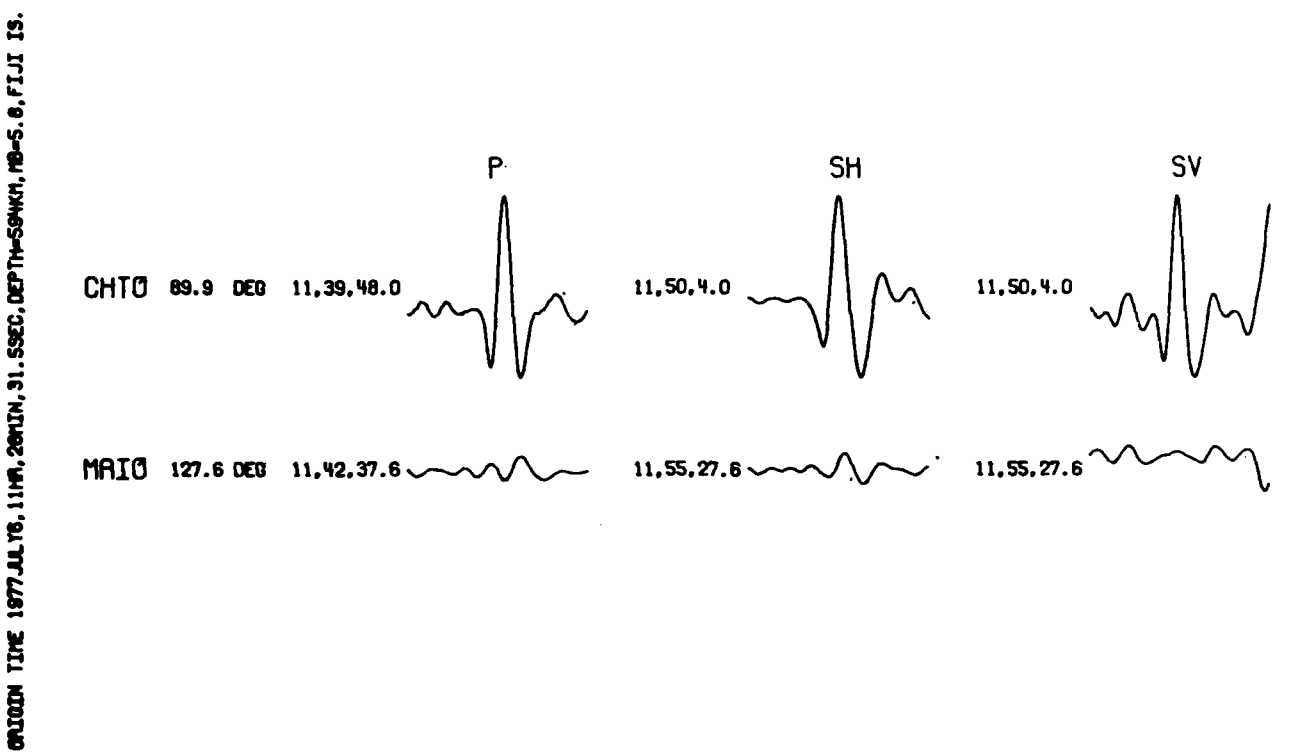

Fig. VI.2.2 Vertical, radial and transverse component SRO records of P, SV, and SH near a great circle path around the core. Time length is 2 minutes.

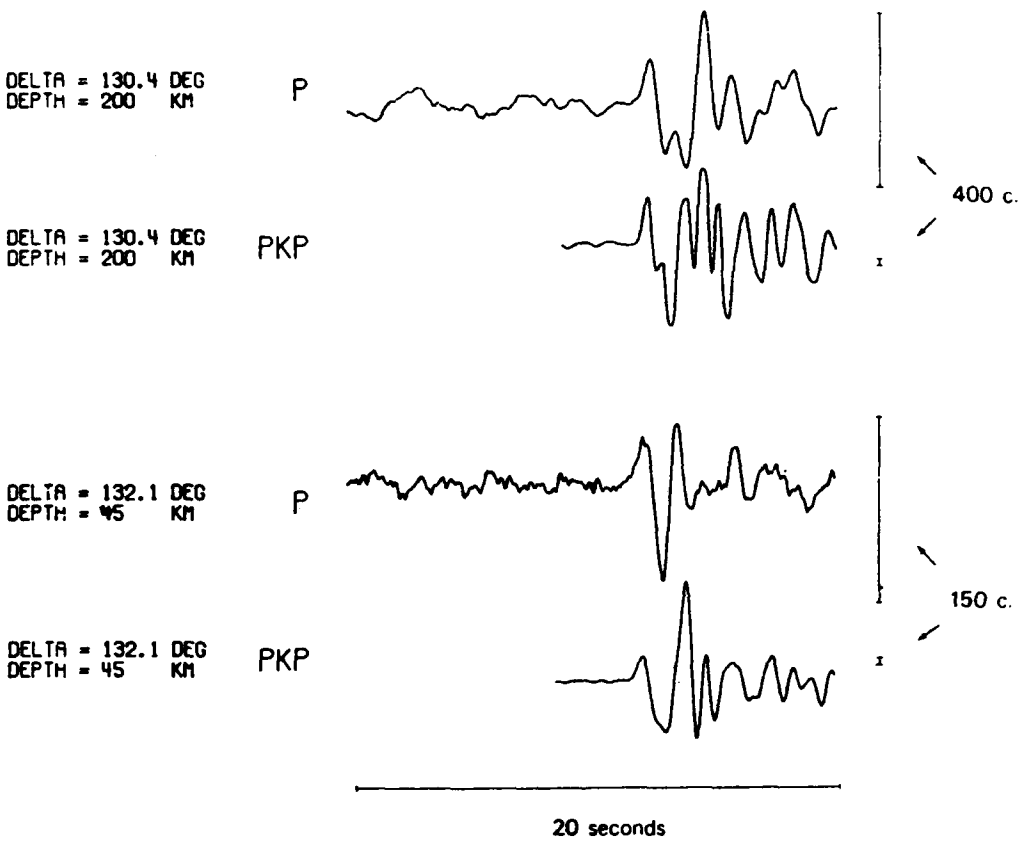

Fig. VI.2.3 NORSAR array beams of short-period P and PKP for two events in the Solomon Islands region (1983, Aug 1 and Nov 30). Time length is 12 seconds.

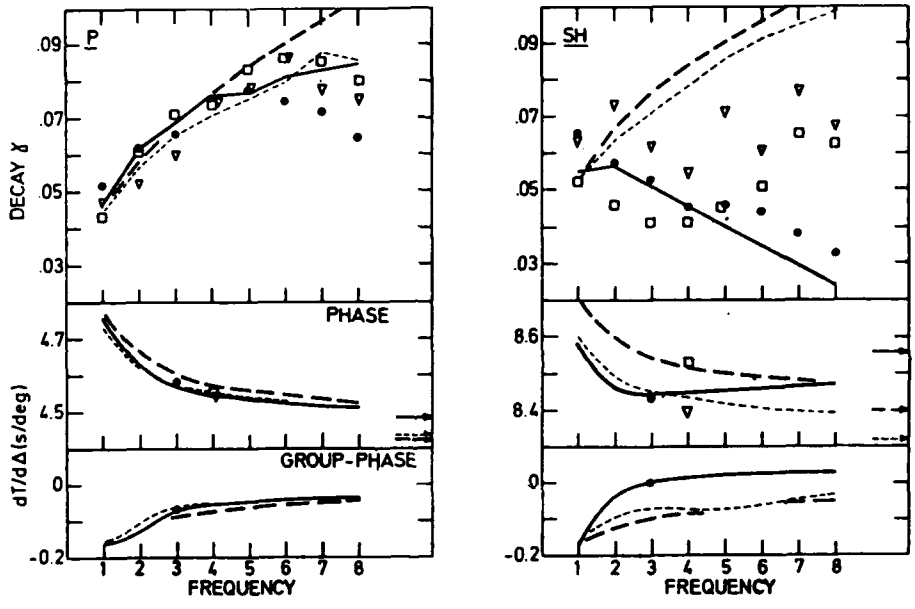

Fig. VI.2.4 Decay spectra and dT/dΔ of P and SH. The decay γ measures logarithmic amplitude decay per degree of epicentral distance and corrected for geometrical spreading. Group-phase slowness is a measure of dispersion. Frequency point 1,...,8 correspond to 0.015625,....,0.125 Hz in steps of 0.015625. Theoretical curves for models ___ ___ : PEM; _____ : PREM; _____ : Ll. Averaged observational data ● : this study; □ and ▽ : other studies.

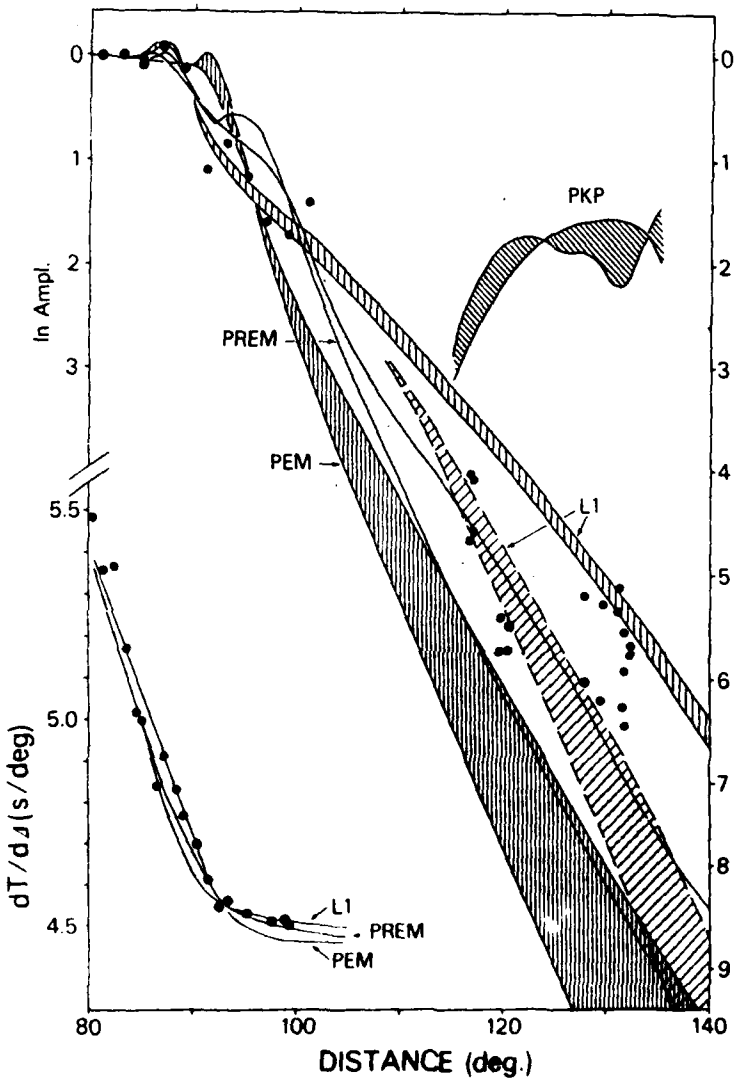

Fig. VI.2.5 dT/dΔ and relative amplitudes of short-period P. Theoretical curves for models PEM, PREM and L1. Amplitude bands correspond to period range 1-2 seconds. Additional amplitude decay due to anelastic damping indicated for model L1 with Q_α = 400 at base of mantle. Amplitude data between 115-135° are from NORSAR (this study). Amplitude and dT/dΔ data between 80-105° are from other studies.

VI.3 The effect of aliasing on the NORSAR detector performance

The standard NORSAR data are recorded with a sampling rate of 20 Hz, but with an anti-aliasing filter at 5 Hz (4.75 Hz to be precise). The reason for this is that the on-line Detection Processing (DP) has always been done at a 10 Hz sampling rate, and the filter has been kept low enough to avoid aliasing problems there.

With the increased interest for regional phases and higher frequencies the question has been raised if the filter could be changed from 5 Hz to 8 Hz, and we have therefore now investigated the effect of this on the on-line detector system. This has been done on the basis of data that have been recorded experimentally with 8 Hz filters at some individual channels. Most of the events analyzed, shown in Table VI.3.1, are taken from a time period in 1978/79 when we had 5 subarray center seismometers equipped with 8 Hz filters (01A00, 02B00, 02C00, 04C00, 06C00), and the rest of the data are from 1982/83, with only 2 '8 Hz channels' in operation.

We have selected events (see Table VI.3.1) from regions with particularly high-frequency signals, which are the signals that presumably should be most affected by aliasing problems as a result of combining 8 Hz filters with 10 Hz processing. The analysis procedure has been as follows:

1. The 17 events in Table VI.3.1 were selected and the data put on disk files.

2. For each event, the data were then plotted as shown on the example in Fig. VI.3.1, with 2 sampling rates (20 and 10 Hz) and 2 filters (1.2-3.2 and 2.0-4.0 Hz). These filter bands are identical to those presently used in NORSAR DP. For comparison, the unfiltered trace was also plotted.

3. For each of the 4 filtered traces, STA/LTA was computed in a way as close as possible to what is done in DP, with options to plot both STA, LTA and STA/LTA traces. The latter ones are shown in Fig. VI.3.2 for the data plotted in Fig. VI.3.1. It is seen from that figure that we do lose some SNR as a result of the decimating process, for the 1.2-3.2 Hz the SNR drops from 3.97 to 3.83 and for the and for the 2.0-4.0 Hz filter from 7.27 to 6.40.

The results for all of the events analyzed are shown in Figs. VI.3.3-4, plotted individually for teleseismic and regional events, and for each of the 2 filters for each event group. We can draw the following conclusions from the figures:

1. For teleseismic events processed at 1.2-3.2 Hz, a change from 5 to 8 Hz anti-aliasing filters would not affect the performance of the 10 Hz DP.

2. For teleseismic events processed at 2.0-4.0 Hz there is a loss in SNR typically around 1-2 dB. For the events analyzed here (and generally for most Eurasian events recorded at NORSAR) this filter band has a significantly better SNR, and a filter change as discussed can therefore not be implemented without a clear negative effect on the DP performance.

3. For regional and local events we see from Fig. VI.3.4 that the scatter in the SNR values is much larger than for the teleseismic events, but with no systematic difference in the SNR range critical for detections. A filter change should therefore not be a problem for these events.

The above analysis has been done on single channels, and it should be expected that the high-frequency beamforming loss should decrease a little the adverse effects of a filter change to 8 Hz. Our conclusion

is nevertheless that an overall change from 5 to 8 Hz anti-aliasing filters should not be implemented unless combined with a change from 10 to 20 Hz processing in DP.

Ø. Pettersen
H. Bungum
F. Ringdal

No.	Date	Region	Arr. Time	(deg)	m_b	NCH	Comments
1	77/12/26	E. Kazakh	04.10.17	38	4.9	5	Expl.
2	78/05/29	E. Kazakh	05.04.17	38	4.7	4	Expl.
3	78/09/20	E. Kazakh	05.10.17	38	4.2	3	Expl.
4	78/12/20	E. Kazakh	04.40.17	38	4.7	4	Expl.
5	79/09/06	C. Siberia	18.07.17	38	4.9	3	Expl.
6	79/09/17	S. Norway	15.22.18	3	2.8	5	Expl.
7	79/09/18	S. Norway	17.56.09	4	2.6	4	Expl.
8	79/09/23	N. Norway	13.54.29	6	3.1	5	
9	79/10/02	S. Norway	14.19.15	3	2.4	4	Expl.
10	79/10/07	C. Siberia	21.08.06	44	4.9	4	Expl.
11	82/12/25	E. Kazakh	04.30.27	39	4.7	2	Expl.
12	83/01/05	Honshu, Japan	07.29.44	71	5.1	1	
13	83/01/07	Honshu, Japan	18.30.32	74	5.1	1	
14	83/02/13	N.W. Kashmir	02.00.55	47	5.1	2	
15	83/02/18	Persian Gulf	07.48.25	47	5.0	1	
16	83/02/20	Hokkaido, Japan	01.32.44	70	5.1	1	
17	83/02/28	Aleutian Isl.	05.44.23	70	5.2	1	

Table VI.3.1 List of events used in analysis of 8 Hz filter aliasing. NCH indicates number of channels analyzed (i.e., number of channels with 8 Hz filters.

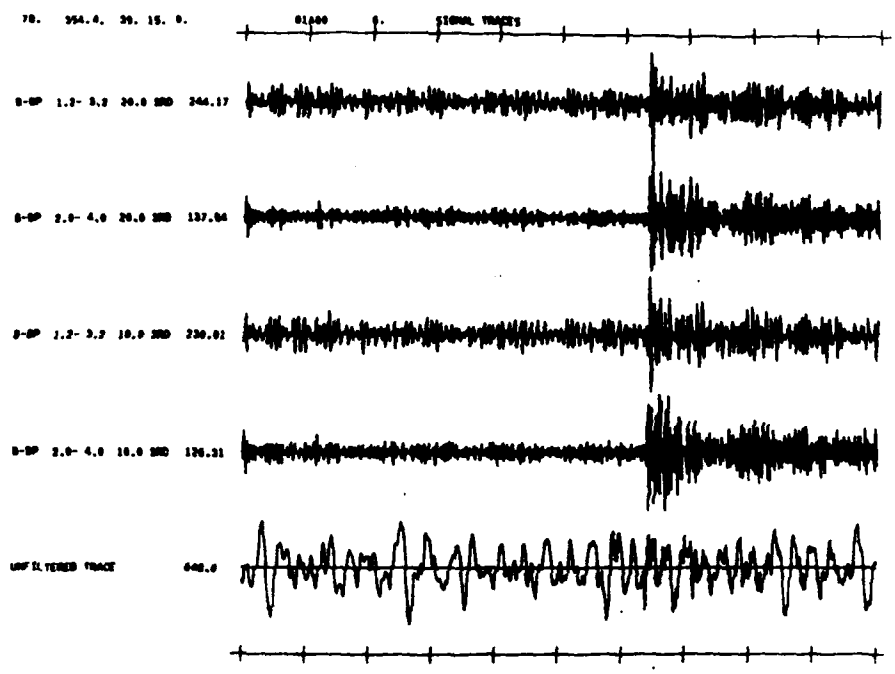

Fig. VI.3.1 Signal traces (100 seconds) for Event 4 in Table VI.3.1, recorded at channel 01A00 with 8 Hz filter and 20 Hz sampling rate. The unfiltered data are shown in the bottom trace, while the first 2 traces show the data filtered 1.2-3.2 Hz and 2.0-4.0 Hz, respectively. Trace 3 and 4 are resampled to 10 Hz and then filtered in the same pass bands. The numbers to the left of each trace are maximum amplitudes, and the traces are scaled individually.

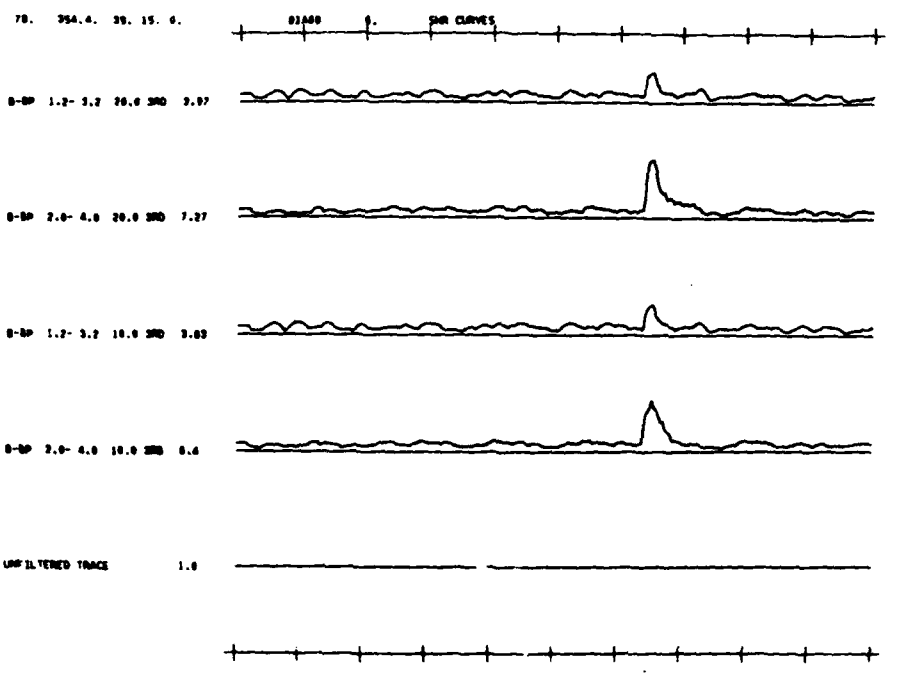

Fig. VI.3.2 SNR (or STA/LTA) curves for the traces plotted in Fig. VI.3.1 (Event 4), i.e., for 2 sampling rates (20 and 10 Hz) and 2 filters (1.2-3.2 and 2.0-4.0 Hz). The numbers to the left of each trace show maximum SNR, and the traces are plotted to the same scale.

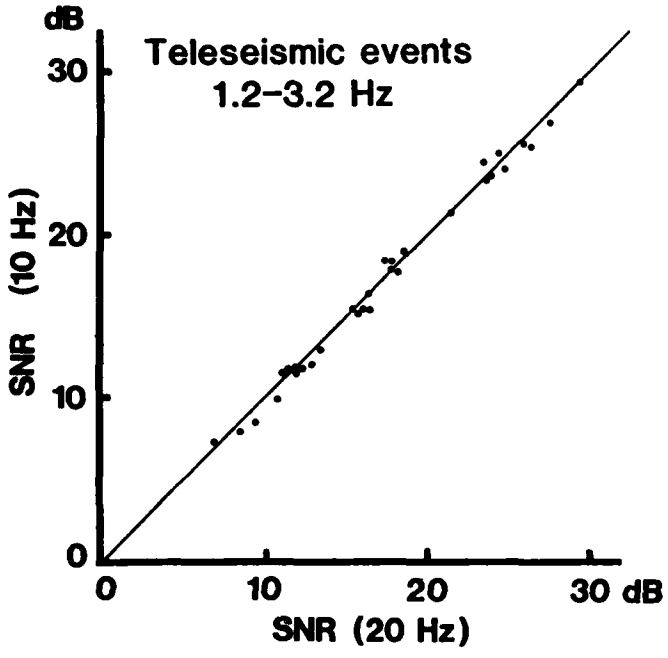

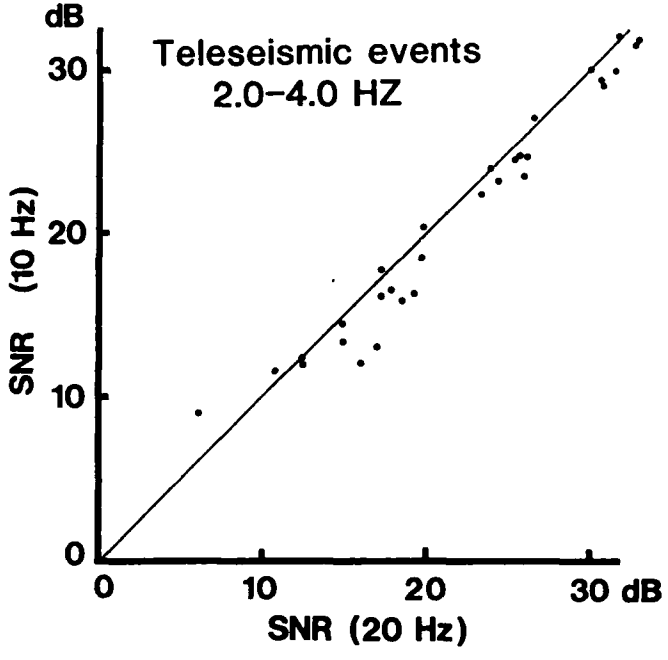

Fig. VI.3.3 SNR (20 Hz) vs SNR (10 Hz) for the teleseismic events (No. 1-5, 10-17) in Table VI.3.1, filtered 1.2-3.2 Hz and 2.0-4.0 Hz.

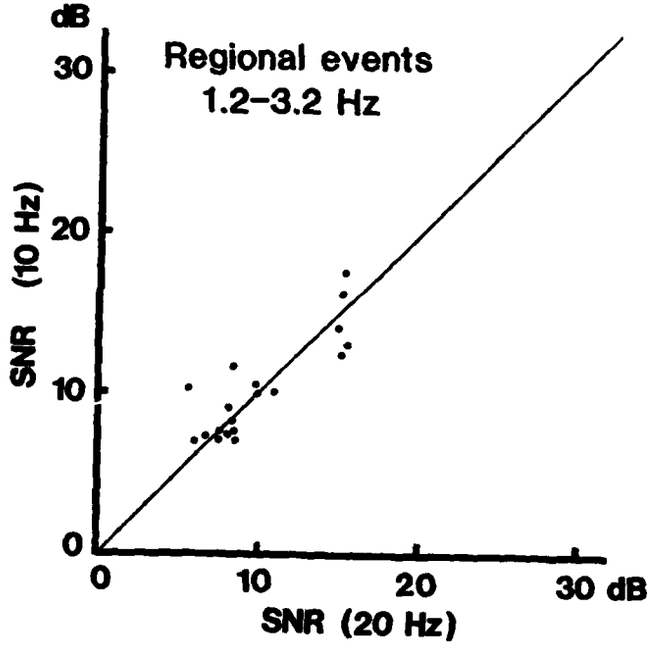

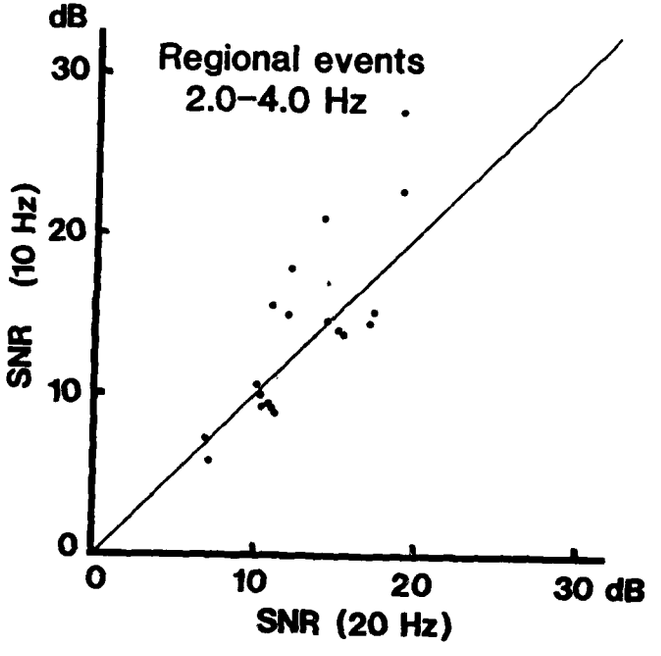

Fig. VI.3.4 SNR (20 Hz) vs SNR (10 Hz) for the regional events (No. 6-9) in Table VI.3.1, filtered 1.2-3.2 Hz and 2.0-4.0 Hz.

VI.4 Seismic noise at high frequencies

Our program for noise measurements in and around the NORSAR siting area, reported upon also in previous Semiannual Reports, has continued in the following way:

- All NORSAR subarrays have been visited with Kinemetrics PDR-2 equipment, 'tapping' the data between the amplifier and the anti-aliasing filter. The sampling rate mostly used has been 62.5 Hz with filter at 25 Hz, but some data have also been recorded with a 125 Hz rate and filter at 50 Hz. This system has an excellent dynamic resolution up to at least 40 Hz.
- The present NORESS area (subarray 06C) has been studied in greater detail (PDR-2 recordings), using both standard 06C sensors and the temporary NORESS sites. Time-of-day variations have also been studied here. Excellent dynamic resolution.
- Data transmitted in analog form to NORSAR from 06C and 02B have also been analyzed, the sampling rate here is 40 Hz, but the dynamic resolution is poor, and there is an increasing amount of system noise from the telephone lines for frequencies above 2-3 Hz.
- Noise data from a 60 m hole have been recorded simultaneously with surface data (using the PDR-2), and comparisons are made under various conditions. Excellent dynamic resolution.
- Six other sites in southeastern Norway have been studied by 'tapping' (using the PDR-2) the analog (telephone) lines from the Southern Norway Seismic Network (SNSN). System noise is a problem also here.

Representative noise spectra from 6 NORSAR subarrays (except 06C) are shown in Figures VI.4.1-2, with recordings using the Kinemetrics PDR-2 on the output from the NORSAR RA-5 amplifiers in the Central Terminal Vault (CTV) of each subarray. This corresponds to System No. 12 in Table III.4.1 of this report, where it is seen that the PDR-2 gives a gain of 42 dB (for the weakest signals) in addition to the 72 dB from the

NORSAR amplifier. The recordings have been done with a sampling rate of 62.5 Hz (16 ms sampling interval) and with an anti-aliasing filter (12 dB/oct) at 25 Hz. The spectra in Figs. VI.4.1-2 cover various parts of the winter from day 337/1982 to day 56/1983 and should therefore be expected to cover generally high noise levels for frequencies below 2 Hz. The 1 Hz levels for the cases shown is between 5 and 10 dB above 1 nm^2/Hz, while we previously have shown that the typical summer level is more in the range 0 to 7 dB. The spectra in Figs. VI.4.1-2 show typical noise levels for each subarray, and it is easily seen that they are strikingly similar (above 2 Hz), with a 10 Hz level at -50 dB below 1 nm^2/Hz. The only exceptional feature in these spectra is a strong 12.5 Hz noise peak from 02C00, that one is caused by inductive interference from a 50 Hz power line close to the analog tranmission line from seismometer to CTV.

From Figs. VI.4.1-2 we can also see for most of the channels some spectral flattening above 15-20 Hz. This is caused by various cultural activities at close distances, and is quite often much more prominent than shown here, sometimes also starting at frequencies as low as 5 Hz. There is a clear correlation between these observations and the population density in the vicinity of each of the subarrays.

Data recorded with a sampling rate of 125 Hz and an anti-aliasing filter at 50 Hz have also been analyzed, as shown in Fig. VI.4.3 for subarrays 02B and 06C (NORESS). It is seen there that the ambient noise level continues to drop at about the same rate all the way up to 50 Hz (provided that cultural noise sources can be avoided), a rate which is close to 15 dB/octave or 50 dB/decade. It is seen that the lowest noise level resolved here is about -80 dB relative to nm^2/Hz, or 260 dB below 1 nm^2/Hz, which is 5 dB below Herrin's (1982) lowest value for Lajitas. The spectral differences between the two sensors in Fig. VI.4.3 are typical, in the sense that subarray 02B is somewhat less affected by cultural noise at high frequencies than 06C, which is the present NORESS site.

Because of the possibility that the 06C area could be chosen as the site also for the permanent NORESS installation, fairly extensive noise surveys have been conducted there. As a part of that, we have covered the area with regular PDR-2 recordings throughout the day and night, and Fig. VI.4.4 shows here an example for 1400, 1800 and 2200 GMT. In addition to the general decrease in the noise level above 5 Hz by night, there is also a prominent and fairly broad peak around 5.5-6.0 Hz which also disappears by night. This peak can also be seen in several of the spectra presented above, and we have come to the conclusion that it probably is caused by the integrated effect of all the traffic in the general area. The survey has moreover shown that the 06C (NORESS) area is at times significantly affected by local cultural noise sources above 5-10 Hz, and much of this comes from lumbering and other economic activities within the immediate vicinity (< 5 km) of the sites. In this sense, both subarray 02B and 03C (which both could be acceptable as NORESS sites from a signal focusing point of view) are somewhat better than 06C, but the difference is not very clear and all seven subarray sites are at times significantly affected by high-frequency cultural noise from sources at short distances.

All the seismic noise spectra presented above have been taken from surface installations (i.e., 2-5 m borehole depths). In order to test the possible gain from deeper borehole installations we have conducted some simultaneous PDR-2 recordings from surface and 60 m deep seismometers at site 01A01, with results as shown in Fig. VI.4.5. It is seen there that the difference starts at around 8 Hz and increases to more than 10 dB for frequencies above 20 Hz. However, in comparing with the 02B and 06C spectra in Fig. VI.4.3 we see that those spectra are closer to the 01A 60 m spectra in Fig. VI.4.5, and we should therefore not expect a gain of this size for sites that are less affected by local cultural noise than 01A. For technical reasons, we have so far not been able to investigate the noise reduction potential for other depths than 60 m.

Seismic noise spectra from 3-component recordings done at subarray 06C are shown in Fig. VI.4.6, using SS-1 seismometers and the usual PDR-2 recorder. The results show that there is no systematic difference between vertical and horizontal components for frequencies above 3-4 Hz, while for lower frequencies the noise level on the vertical component is slightly higher.

We have, in addition to the detailed noise studies from various NORSAR installation, also analyzed data from the Southern Norway Seismic Network (SNSN), in this case also using the PDR-2 recorder in combination with significantly preamplified signals. The results clearly confirm our conclusions from above with respect to the stability of the noise spectra for higher frequencies. However, the data are somewhat affected by transmission noise on the telephone lines used, a problem which also affects our present analog data channels from subarrays 02B and 06C, for frequencies above 2-3 Hz.

In order to facilitate the comparison between a typical NORSAR (or southeastern Norway) noise spectrum and previously published quiet sites, we have in Fig. VI.4.7 plotted our results as presented above on top of the Queen Creek and Lajitas noise spectra (Herrin, 1982). We see from that figure that there is not much difference between these spectra for higher frequencies, and this makes it natural to ask the question if there actually is a fairly stable and uniform ambient noise level globally for these frequencies. In fact, since southeastern Norway and Lajitas (Texas) are so similar (as shown in Fig. VI.4.7), there are no reasons to believe that other areas of the world should be significantly different (provided, of course, that local cultural noise sources can be avoided).

In conclusion, we have found that:

1) The ambient seismic noise level above 2-3 Hz in southeastern Norway is very stable both in time and space. The level at 10 Hz

is always very close to -50 dB relative to 1 nm^2/Hz, with a slope in the 5 to 40 Hz range of 15 dB/octave (50 dB/decade). Levels down to 10^{-8} nm^2/Hz (-80 dB) have been resolved.

2) There is, for all of the sites studied, a problem with cultural noise for frequencies above 5 Hz, and this problem increases with increasing frequency. There is a rush-hour peak around 5.5-6.0 Hz, while the cultural noise above 10 Hz sometimes consists of a broad-band contribution (many sources at various distances) but more often of narrow spectral lines (few and close-in sources). This problem, however, is manageable if careful site surveys are executed.

3) Another prominent cultural noise source consists of inductive interference from nearby 50 Hz power lines, and this often gives significant contributions, especially at 12.5 Hz. We know that most of this interference comes from the cables, but we cannot exclude the possibility of some interference also in the seis-mometer itself if the distance to the power line is small.

4) In comparing the seven subarrays at NORSAR, we find that this 50 Hz (12.5 Hz) noise problem is particularly serious for subarrays 01B and 02C. Subarray 01A is problematic with respect to other cultural noise sources and to some extent also 06C (the present NORESS site), while subarrays 02B, 03C and 04C are somewhat better in this respect, even though these too are somewhat affected by the same problem. This relative rating is consistent with what we should expect from merely looking at the population density and the network of roads in the area.

5) The local cultural noise for frequencies above 8 Hz can be reduced considerably by using 60 m deep boreholes, but we do not know the noise reduction potential for other depths. Wind noise is a small problem in this respect, partly because there usually is very little wind in the area, and partly because most of the wind noise can be

avoided simply by cutting trees near the site and by installing the seismometer at a few meters depth in competent (crystalline) rocks.

6) For higher frequencies there is no systematic difference between vertical and horizontal components.

7) In comparing with so-called 'extremely quiet' sites in other continents (notably Lajitas in Texas) we find that the noise levels there for frequencies above about 10 Hz are quite close to what we find for southeastern Norway. The possibility therefore exists that the ambient noise level that we have found for southeastern Norway, with its stability in time and space, in fact could be a globally representative noise level.

H. Bungum

Reference

Herrin, E.T. (1982): The resolution of seismic instruments used in treaty verification research. Bull. Seism. Soc. Am. 72, S61-S67.

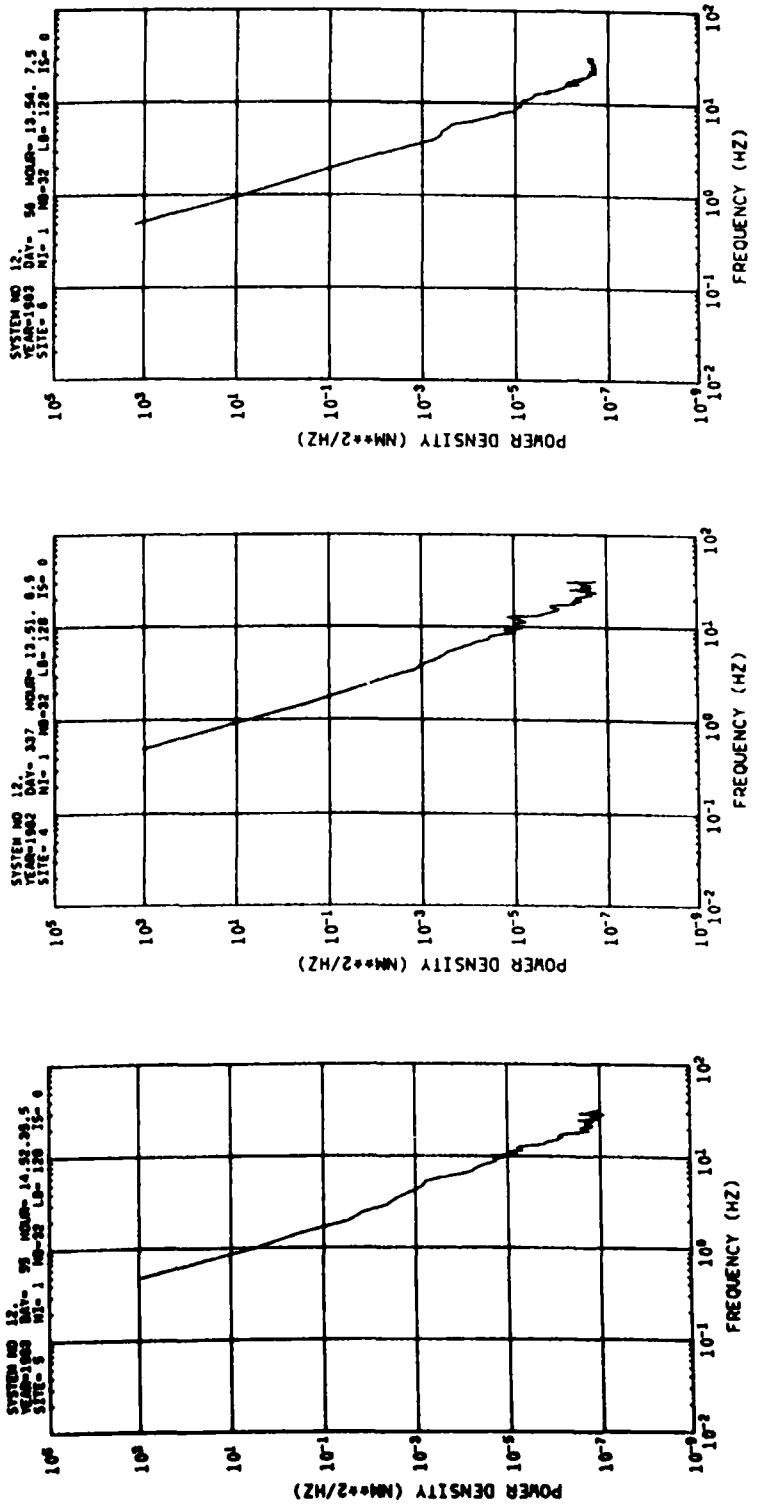

Fig. VI.4.1 Noise power spectra (PDR-2 recording at 62.5 Hz) for NORSAR site 01A05 (left, day 55/1983), 01B04 (center, day 337/1982), and 02B00 (right, day 56/1983). All are day-time spectra.

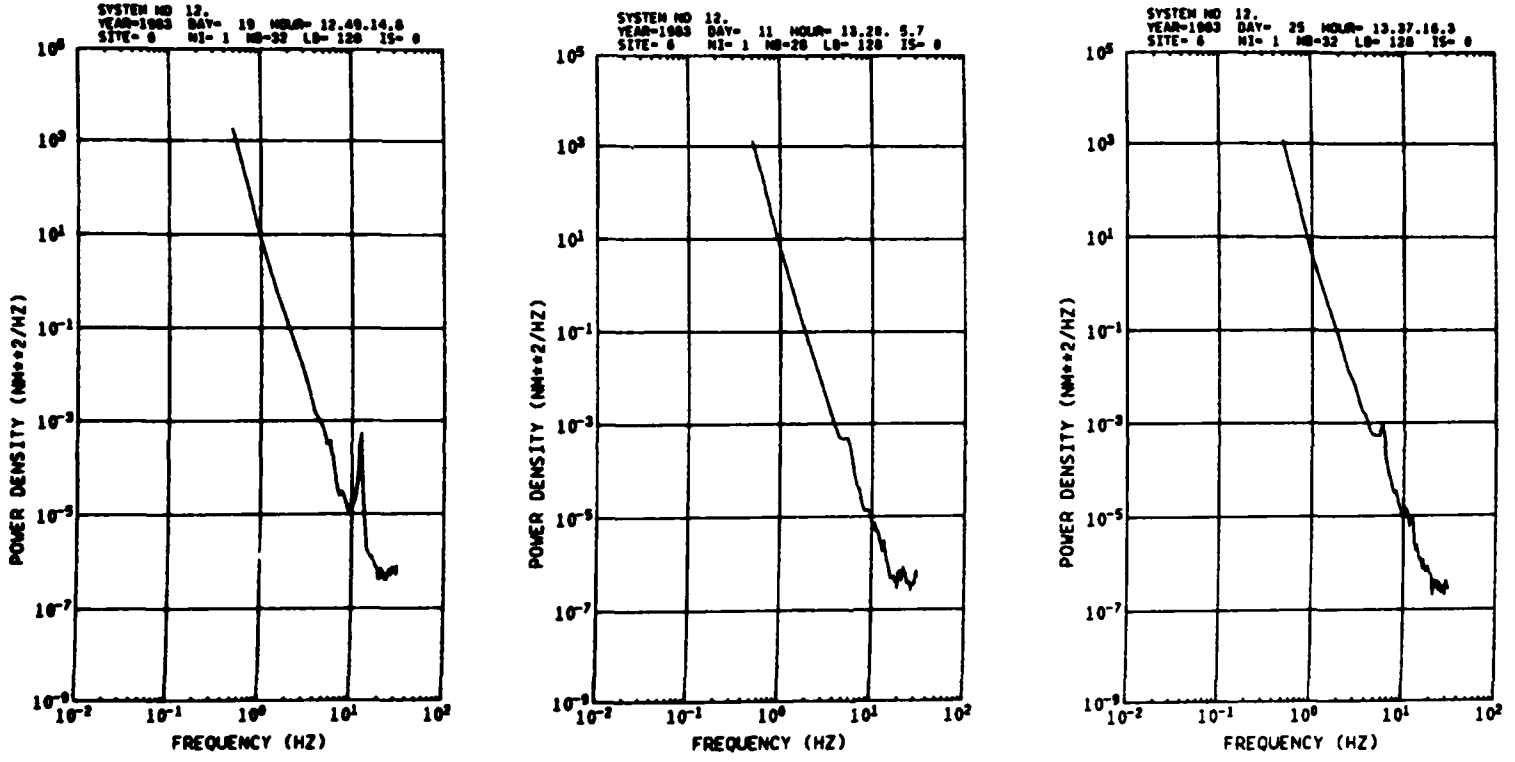

Fig. VI.4.2 Noise power spectra (PDR-2 recording at 62.5 Hz) for NORSAR site 02C00 (left, day 19/1983), 03C00 (center, day 11/1983), and 04C00 (right, dat 25/1982). All are day-time spectra.

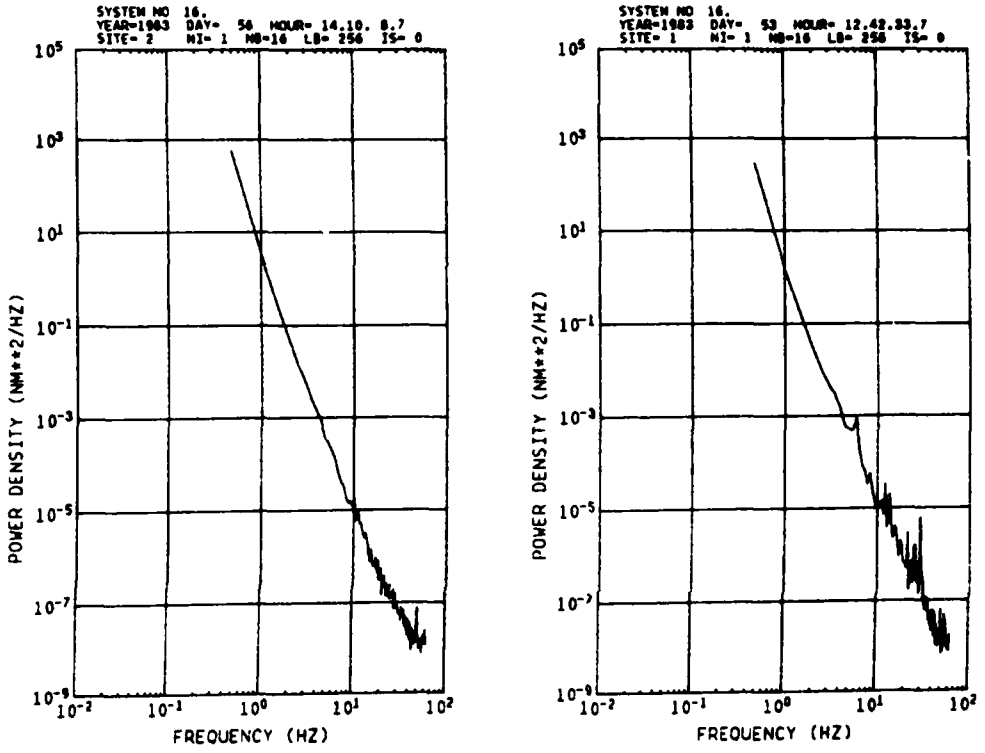

Fig. VI.4.3 Noise power spectra (PDR-2 recording at 125 Hz) for NORSAR site 02B00 (left, day 56/1983) and 06C02 (right, day 53/1983). Both are day-time spectra.

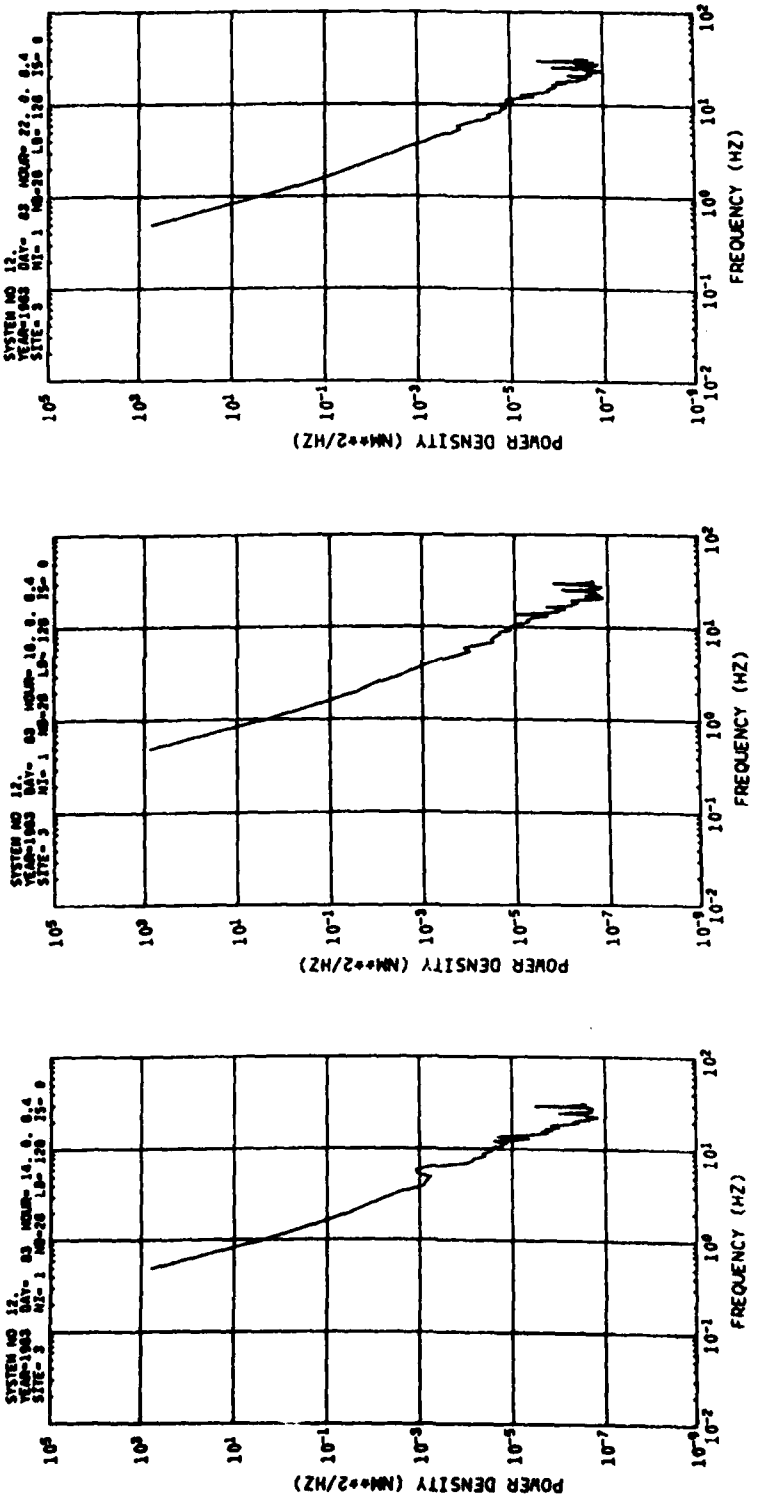

Fig. VI.4.4 Noise power spectra (PDR-2 recording at 62.5 Hz) for NORESS Site 8 (close to 06C02) from day 83/1983 at 1400, 1800 and 2200 GMT.

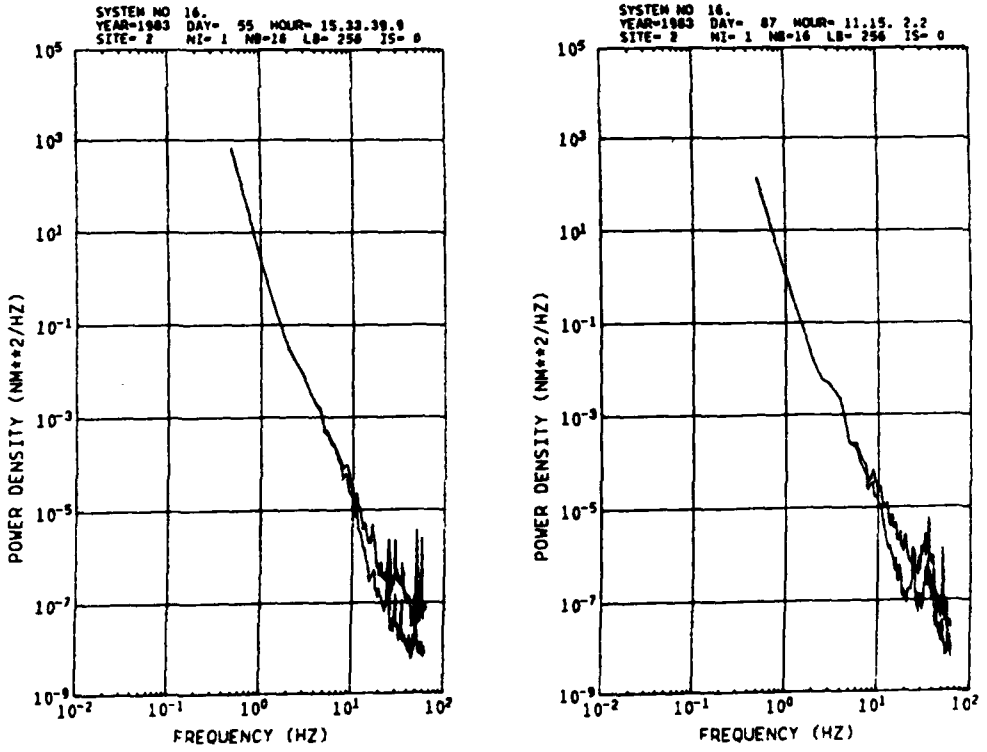

Fig. VI.4.5 Noise power spectra (PDR-? recording at 125 Hz) for NORSAR Site 01A01 and from a 60 m borehole at the same site, at two different times (day 55/1983 and day 87/1983).

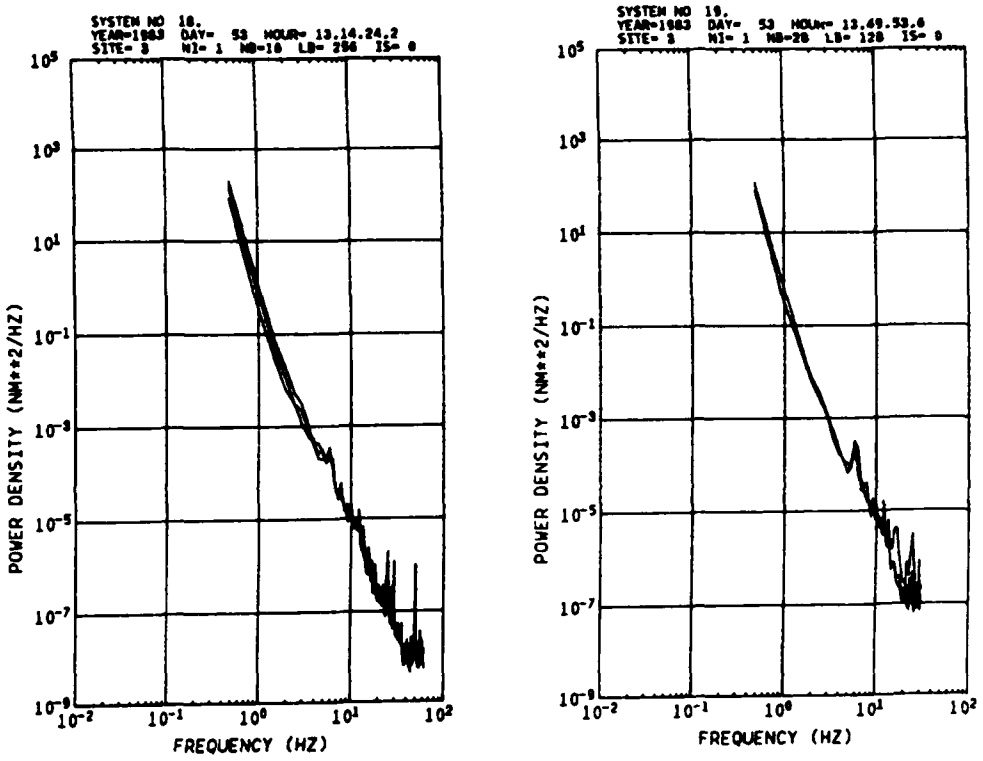

Fig. VI.4.6 Noise power spectra (PDR-2 recording) for NORSAR Site 06C02, using 3-component SS-1 seismometers, day 53/1983. Both are day-time spectra, left: 1314 GMT, 125 Hz recording; right: 1349 GMT, 62.5 Hz recording.

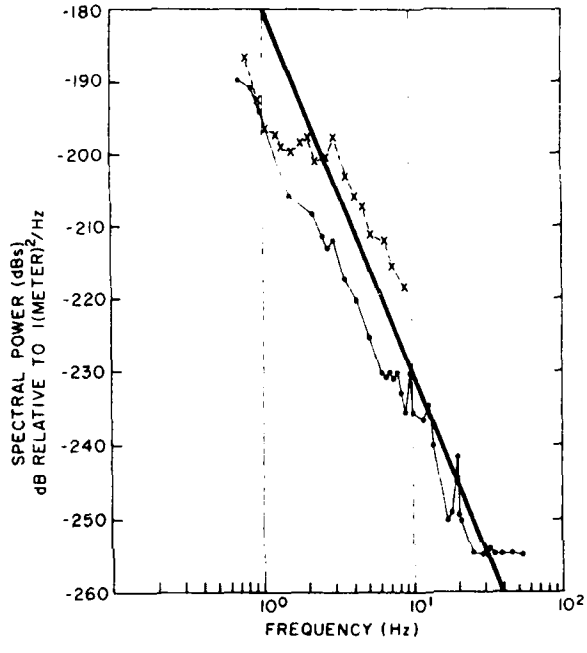

Fig. VI.4.7 Noise power spectra for 1) Lajitas (dots), 2) Queen Creek (x's) and 3) southeastern Norway (heavy line). 1) and 2) are taken from Herrin (1982) while 3) is a typical average for the data presented in this study (for frequencies above 2 Hz).

VI.5 Power spectral bias sources and quantization levels

In seismic data acquisition systems there are three main sources of non-seismic noise (system noise) causing various kinds of limitations in resolution and dynamic range:

1. The seismometer/amplifier system

2. The transmission system (modulators/demodulators, telemetry equipment, telephone lines, etc.)

3. The recording system, for digital systems mainly quantization errors.

A typical problem associated with the Type 1 noise source is given a seismometer/amplifier system with a certain dynamic range, to find a gain level that gives a reasonable tradeoff between the conflicting needs for resolving the seismic background noise and at the same time avoiding clipping of strong signals. This is a particular problem with regional and local earthquake data as the necessary dynamic range for these signals is significantly larger than for teleseismic events.

We have at times experienced significant problems associated with the Type 2 noise source when using leased telephone lines for data transmission on analog form. This applies in particular to systems 9, 13 and 14 described in Section III.2, where we have found (for the particular amplifier gain used there) that the system noise is approximately white and that it reaches the level of the ambient background noise at a frequency of 4-5 Hz, causing an increasing amount of spectral bias for higher frequencies.

For many seismic systems the main limiting factor with respect to dynamic resolution is the limitations within the recording system (Type 3 errors) more than those of the seismometer/amplifier system. For digital systems, the main limitation is the number of bits available for representation of signal level. This problem is sometimes 'solved' by gain-ranging

(increasing the quantization step with increasing signal level), which works well as long as the signal spectrum is reasonably white and/or band-limited in frequency. However, the real situation with seismic signals (including earth noise) is that weak high-frequent signals are superimposed on strong low-frequent ones, and quantization errors are therefore dependent upon the shape of the noise and signal spectra (for a discussion of quantization errors under simpler conditions, see Oppenheim and Schafer, 1975).

We have addressed the problem of quantization errors in a strictly empirical way, starting with the unbiased earth noise spectra presented in Section VI.4. Three different power spectra were selected, where the main difference was that they were based on data sampled at 125, 62.5 and 40 Hz, with filters at 50, 25 and 12.5 Hz, respectively (corresponding to systems 16, 12 and 17 in Section III.4). Each of the (integer) time series were then scaled down successively by factors of two, and the power spectra calculated. The results are given in Fig. VI.5.1, where four power spectra are calculated:

1) Scaling factor 2^0, with 0.000334 NM/QU at 1 Hz
2) Scaling factor 2^8, with 0.0855 NM/QU at 1 Hz
3) Scaling factor 2^{10}, with 0.342 NM/QU at 1 Hz
4) Scaling factor 2^{12}, with 1.37 NM/QU at 1 Hz

It is seen from the figure that the power spectra for 1) and 2) overlap almost completely (all possible effects of the PDR-2 gain-ranging have been removed by a scaling of 2^7), at quantization level 3) there is a clear bias extending in the worst case almost down to 10 Hz, while for level 4) the bias extends to about 5 Hz. For these and similar curves we have derived the relationship shown in Fig. VI.5.2, which shows the minimum quantization level that is required for resolving earth noise at a particular frequency, provided that the anti-aliasing filter is above the frequency considered. It must be emphasized here that this relationship

is dependent upon the earth noise power spectrum as well as upon the system response function. If used as a guideline for choosing quantization levels, it would be wise of course to select a level a factor of two better than the minimum requirement.

The results presented above can be used also for investigating the limits in resolution for the standard NORSAR system, which (see also Section III.4) have the following very severe gain-ranging:

1) Sample range 1-127, quantization 0.0427 NM/QU
2) Sample range 128-511, quantization 0.171 NM/QU
3) Sample range 512-2047, quantization 0.683 NM/QU
4) Sample range 2048-8191, quantization 2.73 NM/QU

We find at NORSAR that the peak amplitudes of the seismic background noise are usually at sample range 2) but occasionally at range 3), which means that the quantization is either 4 or 16 times poorer than indicated by the usually quoted value of 0.0427 NM/QU. In order to test this on real data we have in Fig. VI.5.3 computed three noise power spectra covering the same time interval, with 1) unbiased PDR-2 data, 2) NORSAR data filtered at 8 Hz, and 3) NORSAR data filtered at 4.75 Hz. These filters are very sharp (24 dB/octave), and we can never recover unbiased data above the cutoff frequency. In fact, from Fig. VI.5.3 we see that the bias in the worst case may extend down to between 3 and 4 Hz. However, the data used in Fig. VI.5.3 are taken from different channels causing some level differences also for lower frequencies, and it is therefore not possible to find a more exact 'bias frequency' from such tests (there are also some instabilities in time).

Another implication of the results presented here is that an even stronger bias should be expected for earthquake and explosion signals with peak amplitudes in sample range 3) and a sharp rolloff in the spectrum towards higher frequencies.

The best way to solve these problems would of course be to replace the AD-converter with a more advanced one (increasing significantly the number of bits), but some improvement (for small signals) within the frame of the old system could also be obtained by whitening the uncorrected power spectrum through the introduction of an extra analog high-pass filter (with a reasonably gentle slope).

H. Bungum

Reference

Oppenheim, A.V. and R.V. Schafer (1975): Digital Signal Processing (Chapter 9), Prentice-Hall, New Jersey.

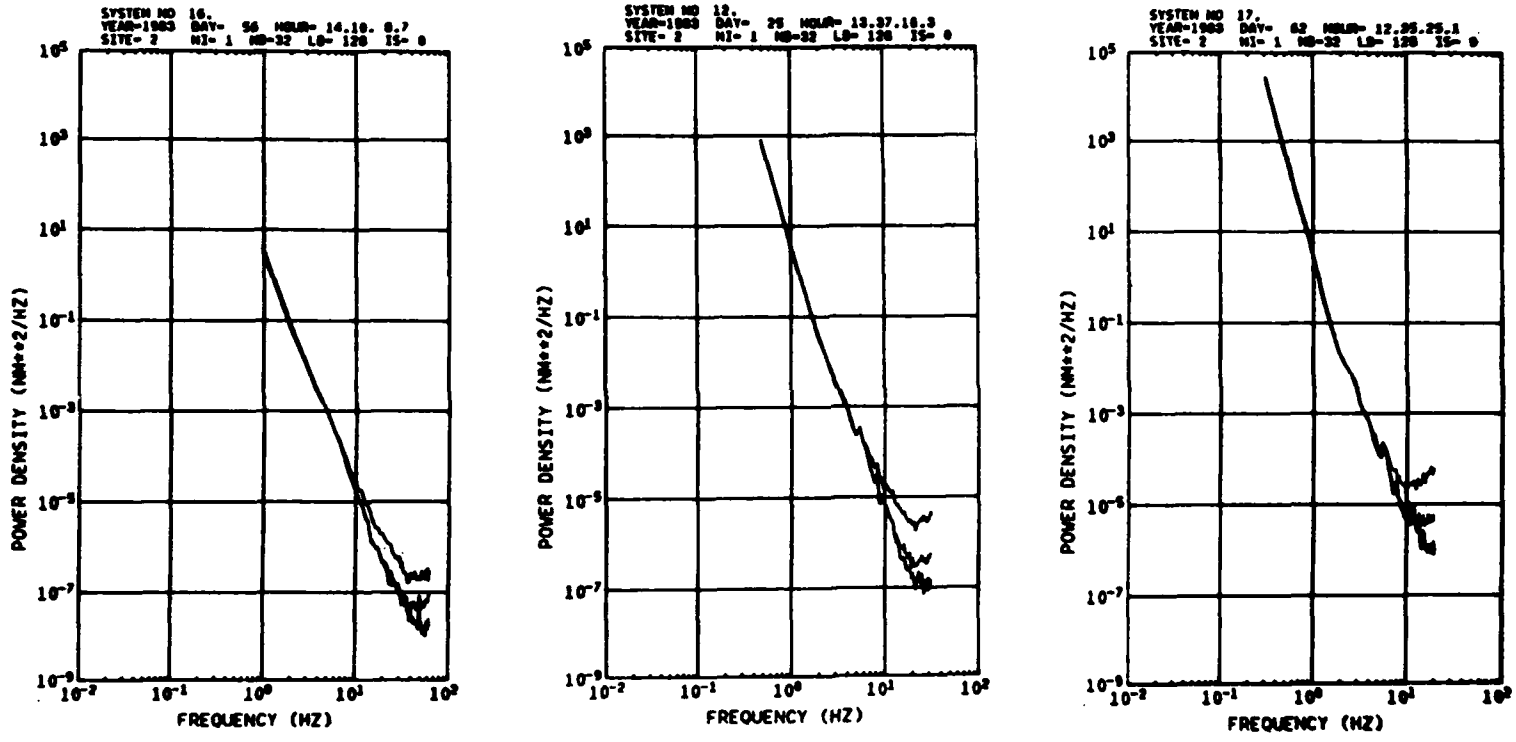

Fig. VI.5.1 Noise power spectral for left: day 56/1983 (125 Hz sampling, 50 Hz filter), center: day 25/1983 (62.5 Hz sampling, 25 Hz filter), right: day 62/1983 (40 Hz sampling, 12.5 Hz filter). For each day, spectra are computed at 4 different quantization levels: 1) original data (PDR-2 recording at NORSAR subarray) with at most 0.000334 nm/Qu at 1 Hz; 2) same data scaled down to 0.0855 nm/Qu (overlapping trace 1); 3) scaled to 0.342 nm/Qu (center trace); and 4) scaled to 1.37 nm/Qu (uppermost trace, strongly biased).

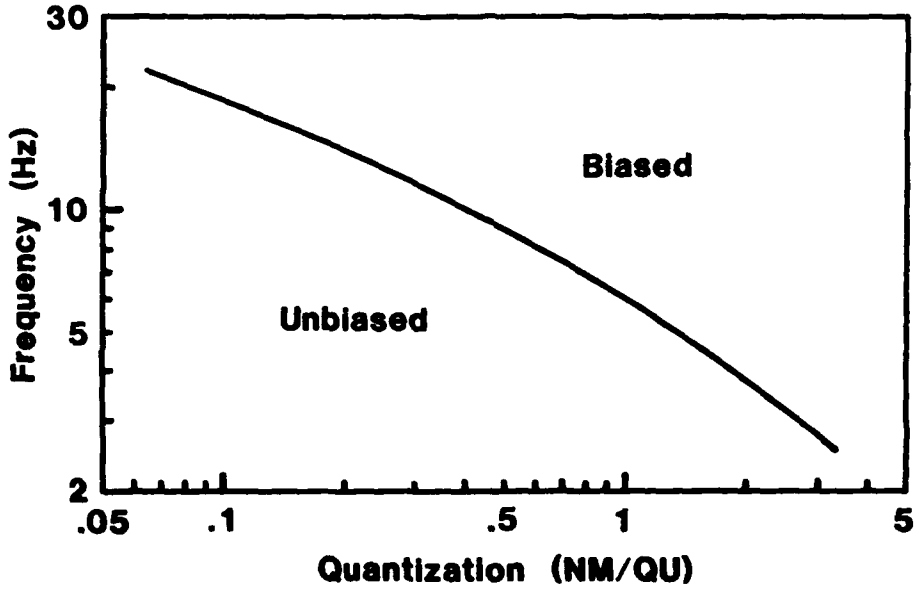

Fig. VI.5.2 Relationship showing the frequency range for which sufficient noise resolution can be obtained (unbiased spectra), given a certain quantization level at 1 Hz. The relationship is valid only for the particular combination of noise power spectrum observed in southeastern Norway (see Section VI.4) and the response functions of the systems used to delineate it (see Section III.4, systems 12, 16 and 17).

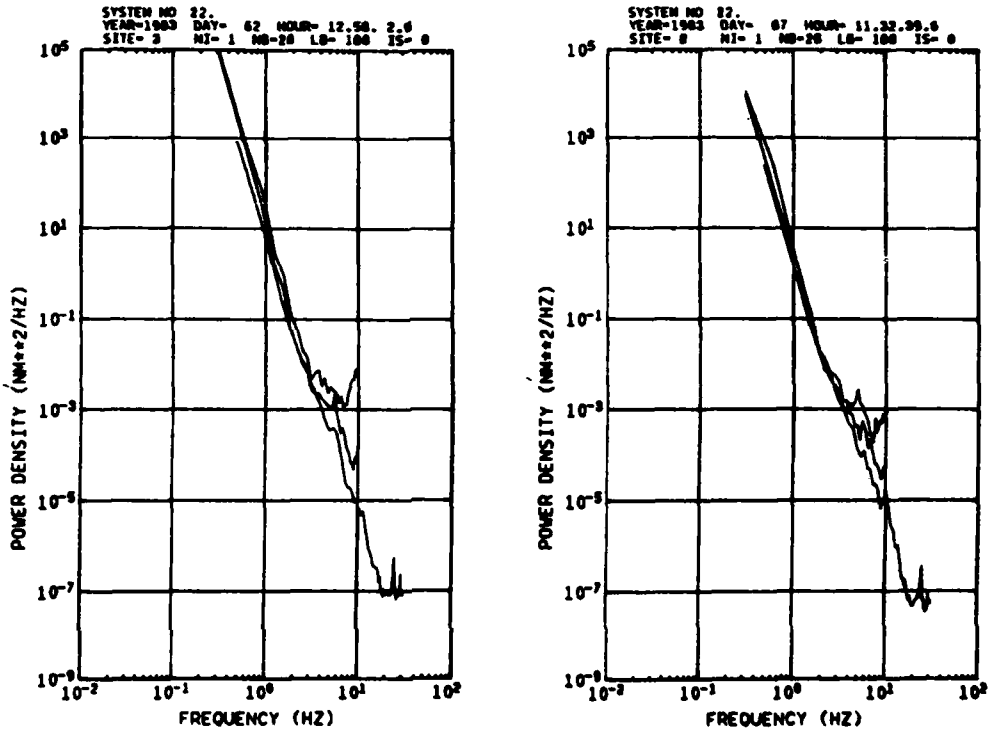

Fig. VI.5.3 Noise power spectra for day 62/1983 (left), and day 87/1983 (right), and with each case covered by: 1) an unbiased PDR-2 recording with sufficient quantization (62.5 Hz sampling rate, 25 Hz filter); 2) NORSAR 20 Hz recording with 8 Hz filter (center trace); and 3) NORSAR 20 Hz recording with 5 Hz filter (top trace, clearly biased).

VI.6. Magnitudes from P coda and Lg using NORSAR data

The objective of this study is to investigate the stability of magnitude estimates based on P coda and Lg, compared to that of conventional P-wave magnitudes. Using NORSAR recordings of presumed explosions from Semipalatinsk as a data base, the purpose has been in particular to evaluate amplitude variations across the array as well as compare NORSAR magnitude estimates to those of ISC and NEIS.

For the purpose of this study, NORSAR recordings of 25 presumed explosions from Semipalatinsk (Table VI.6.1) were used as a data base. The epicentral distance is about 38 degrees for these events, and Lg is usually only slightly stronger than the preceding P coda (Fig. VI.6.1). It is noteworthy that the coda energy stays significantly above the noise level for several minutes following Lg, in the case of high magnitude events. However, we have found that below m_b = 5.5 the noise influence on the Lg arrival becomes significant except during very quiet noise conditions.

We will first consider the amplitude variations across NORSAR for a given event. The significant variability of P amplitudes across NORSAR is well known, as illustrated in Fig. VI.6.2. The standard deviation is frequency dependent, and typically ranges from about 0.20 to 0.25 m_b units. Furthermore, the amplitude pattern is strongly regionally dependent (Berteussen and Husebye, 1974; Ringdal, 1977). Fig. VI.6.3 shows that the variability of the P coda is significantly lower (between 0.07 and 0.10 m_b units standard deviation of peak amplitudes in 30 second windows using a 0.6-3.0 Hz filter) and in fact remains fairly constant out to and beyond the Lg arrival. Furthermore, the variability of the P coda across NORSAR is similar to that of the noise preceding P, if equal time windows are used. If RMS values are considered, the standard deviations are slightly lower, and average about 0.06 m_b units.

We may therefore conclude that considering P coda or Lg reduces the receiver 'focusing' effects in the sense that the standard deviations across NORSAR are reduced by a factor between 2 and 3 compared to the first few cycles of P.

The near receiver 'focusing' effects observed for P-waves across NORSAR might be expected to have counterparts in near-source 'focusing'. Although the actual physical interpretation is uncertain, it is nevertheless clear that significant regionally dependent bias values are observed at NORSAR even within a very limited source area. Fig. VI.6.4 shows NORSAR m_b plotted against ISC m_b (or NEIS m_b where ISC data are not available). The most noteworthy feature is the consistently low NORSAR magnitudes for Degelen Mountains events compared to events from Shagan River. However, there is considerable variability even within the latter region. For the entire event set, the NORSAR bias (at instrument 01A04) varies from 0.0 to about 0.7 m_b units, with a mean of 0.42 and a standard deviation of 0.21. Since the amplitude pattern across NORSAR is fairly stable for Semipalatinsk events, these relative bias values remain also when averaging magnitudes across the NORSAR array.

Fig. VI.6.5 is similar to Fig. VI.6.4, except that NORSAR m_b is replaced by log RMS Lg amplitudes at NORSAR. The standard deviation is reduced to 0.10 logarithmic units, i.e., about half of that obtained using conventional m_b. Furthermore, the Degelen Mountain events now fall into the general trend of Shagan River events. As shown in Figure 6, the scatter between average and single instrument Lg observations is small.

We can conclude that magnitudes based on Lg effectively reduce bias due to near-receiver as well as near-source effects. The question of how accurately m_b estimates can be obtained using Lg from a single station (or an array) for a region like Semipalatinsk remains open, but it seems reasonable that the standard deviation of 0.10 m_b units represents an upper bound. Indeed, it is quite common that m_b estimates by NEIS and ISC differ by 0.1 m_b units or more, even though many of the same stations are used. Furthermore, about half of the stations used in these estimates are located in Central Europe, thus implying that the NEIS and ISC estimates may be severely biased because of the lack of homogeneous geographical station distribution. Thus it is quite possible that single station m_b (Lg) magnitudes may have an accuracy at least as good as those of NEIS

or ISC. Additional improvements may of course be obtained by averaging Lg magnitudes from a well-distributed network of stations.

F. Ringdal

References

Berteussen, K.-A. and E.S. Husebye (1974): Amplitude pattern effects on NORSAR P-wave detectability, NTNF/NORSAR Sci. Report No. 1, 1974/75.

Ringdal, F. (1977): P-wave amplitudes and sources of scattering in m_b-observations, J. Geophys. 43, 611-622.

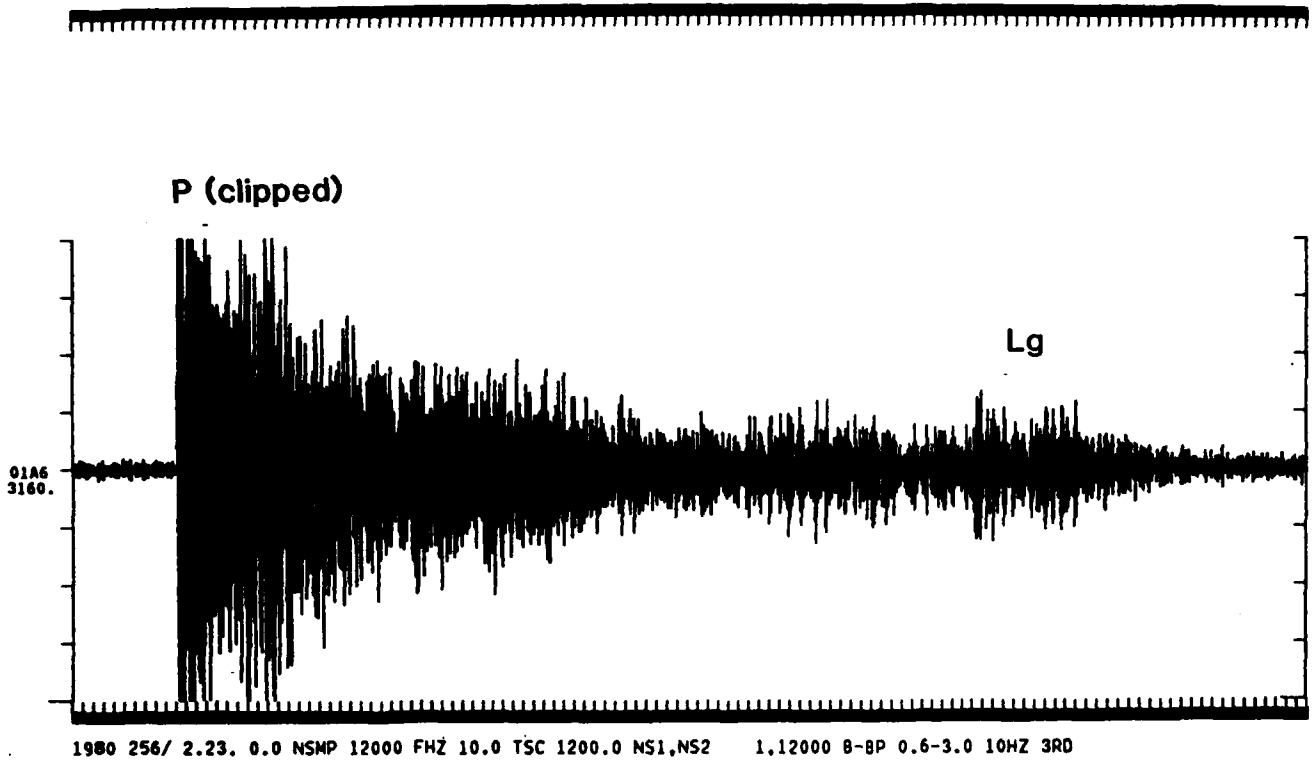

Fig. VI.6.1 Recordings on NORSAR instrument 01A06 for Event 22 of Table VI.6.1. The figure covers 20 minutes, and the data have been filtered in the band 0.6-3.0 Hz. For illustration purposes, the P signal has been clipped on the plot. Note that the P coda level exceeds the noise preceding P for the entire time window, and also that Lg is only slightly larger than the preceding P coda.

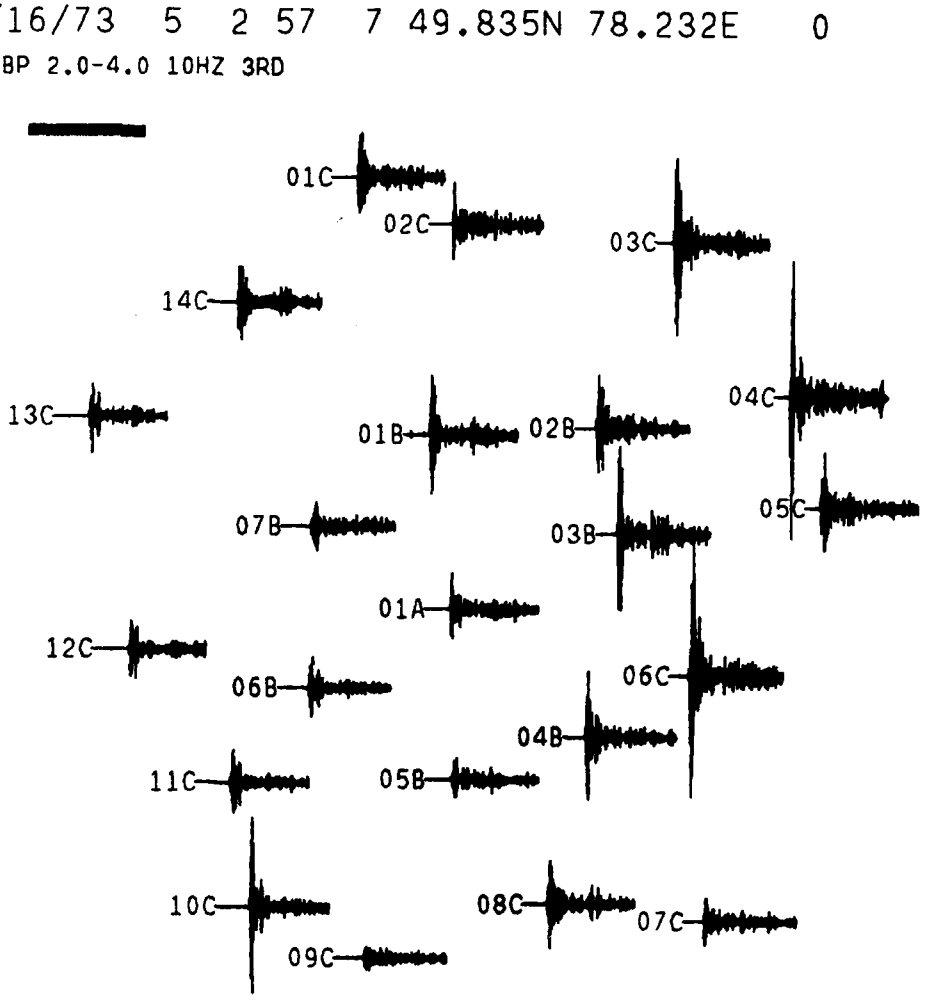

Fig. VI.6.2 Typical P-wave amplitude distribution across NORSAR for Semipalatinsk events. The figure covers 30 seconds of filtered SP data (2-4 Hz) for each center sensor of the 22 NORSAR subarrays. Amplitudes vary by a factor of 10 for the initial P onset, whereas the amplitude variation is less pronounced in the P coda.

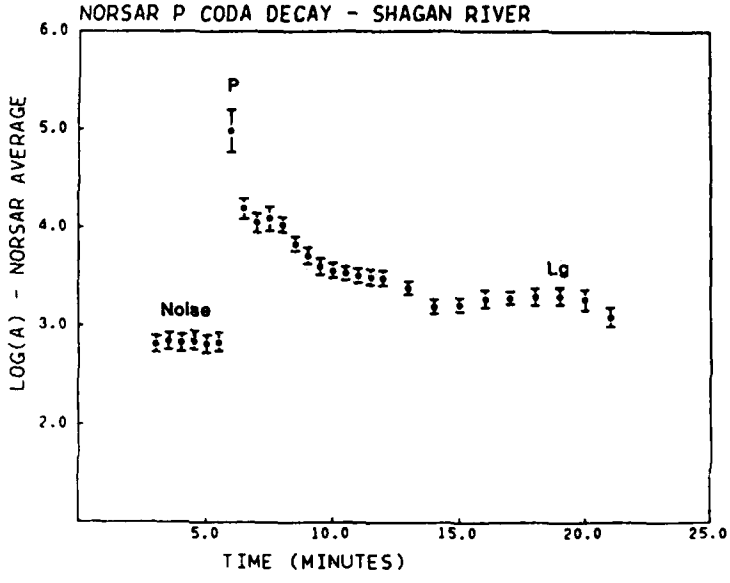

Fig. VI.6.3 Typical P coda decay of NORSAR recordings from Shagan River events. The standard deviations of peak amplitudes across NORSAR in 30 second windows are indicated by vertical bars. Data for the plot has been obtained by combining Events 2 and 8 of Table VI.6.1, and a filter of 0.6-3.0 Hz has been applied.

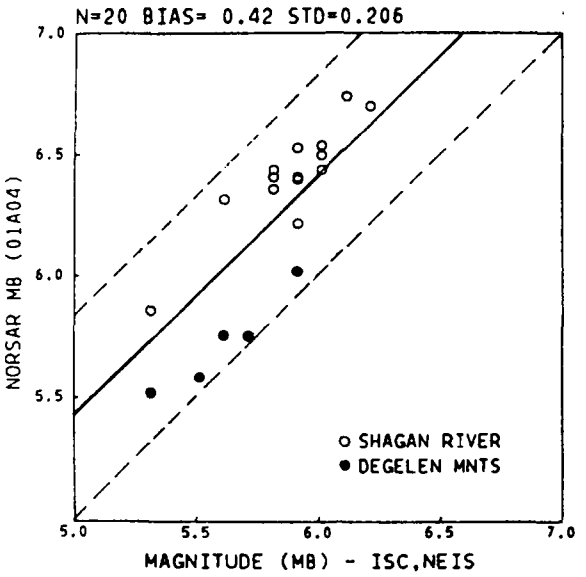

Fig. VI.6.4 NORSAR m_b (instrument 01A04) versus ISC or NEIS m_b (ISC data used when available). Note the difference in m_b bias between events from Shagan River and Degelen Mountains. The stippled lines correspond to plus and minus two standard deviations.

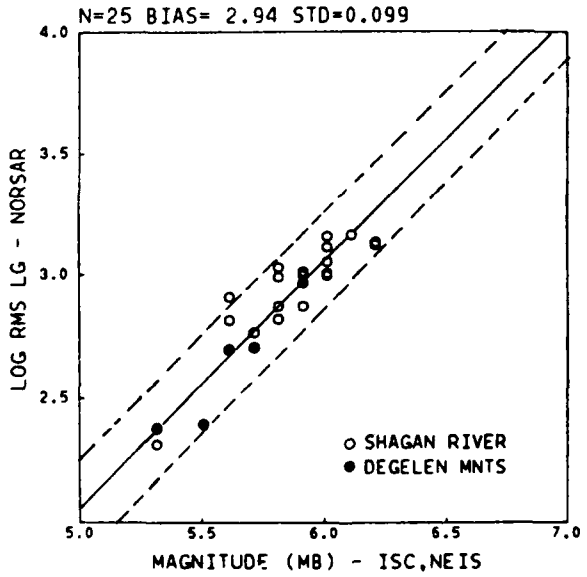

Fig. VI.6.5 Same as Fig. VI.6.4, except that NORSAR m_b has been replaced by an Lg energy estimate. This estimate has been obtained by averaging log RMS of individual NORSAR sensor traces filtered in the band 0.6-3.0 Hz. The time window is 2 minutes, starting 40 seconds before Lg arrival. Note that Shagan River and Degelen Mountain events now show good consistency.

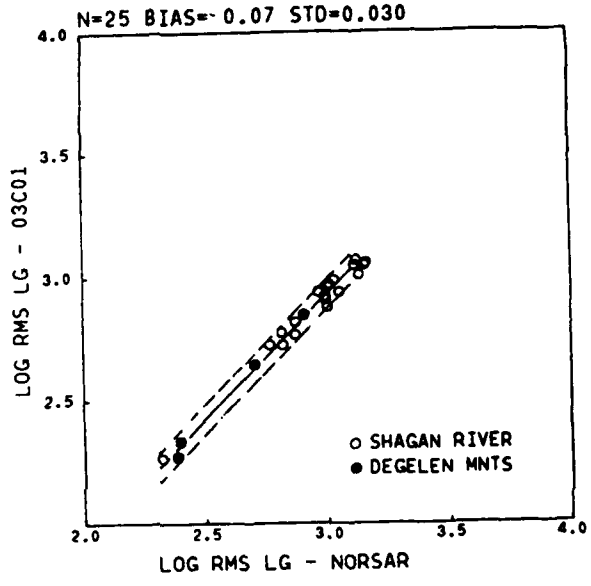

Fig. VI.6.6 Comparison of single sensor Lg energy estimate (subarray 03C, instrument 1) to the average values across NORSAR.

EVENT	DATE	OR. TIME	LAT	LON	MB NEIS	MB ISC	MB NORSAR	LOG LG ARRAY	STD	LOG LG 03C1
1	05/29/77	02 56 57	49.944N	78.846E	5.6	5.8	6.34	2.80	0.065	2.71
2	06/29/77	03 06 57	50.034N	78.927E	5.3	5.3	5.84	2.30	0.053	2.25
3	09/05/77	03 02 57	50.092N	78.961E	5.9	5.8	6.42	2.98	0.070	2.90
4	04/25/71	03 32 57	49.823N	78.092E	5.9	5.9	6.00	2.95	0.057	2.92
5	03/26/78	03 56 57	49.734N	78.074E	5.5	5.6	5.74	2.68	0.053	2.63
6	04/22/78	03 06 57	49.720N	78.175E	5.3	5.3	5.50	2.36	0.05E	2.26
7	06/11/78	02 56 57	49.879N	78.838E	5.9	5.9	6.38	2.86	0.061	2.80
8	07/05/78	02 46 57	49.839N	78.906E	5.8	5.8	6.34	2.85	0.056	2.75
9	07/28/78	02 46 57	49.744N	78.168E	5.7	5.7	5.74	2.69	0.058	2.63
10	09/15/78	02 36 57	49.898N	78.925E	6.0	6.0	6.48	2.98	0.064	2.90
11	11/04/78	05 05 57	50.046N	78.983E	5.6	5.6	6.30	2.89	0.056	2.83
12	06/23/79	02 56 57	49.918N	78.915E	6.3	6.2	6.68	3.12	0.054	2.99
13	07/07/79	03 46 57	50.053N	79.065E	5.8	5.8	6.39	3.02	0.067	2.97
14	08/04/79	03 56 57	49.901N	78.959E	6.1	6.1	6.72	3.15	0.059	3.04
15	10/28/79	03 16 56	49.967N	79.060E	6.0	6.0	6.42	3.10	0.064	3.03
16	12/02/79	04 36 57	49.894N	78.843E	6.0	6.0	6.52	2.99	0.067	2.94
17	05/22/80	03 56 57	49.729N	78.100E	5.5	5.5	5.97	2.38	0.048	2.32
18	06/29/80	02 32 57	49.920N	78.849E	5.7	5.7	-	2.75	0.04E	2.71
19	10/12/80	03 34 14	49.958N	79.085E	5.9	-	6.20	2.99	0.067	2.86
20	12/14/80	03 47 06	49.932N	79.005E	5.9	-	6.39	3.00	0.052	2.95
21	04/22/81	01 17 11	49.901N	78.901E	5.9	-	6.51	2.98	0.043	2.89
22	05/13/81	02 17 18	49.882N	78.971E	6.0	-	-	3.14	0.075	3.03
23	10/18/81	03 57 02	49.891N	78.877E	6.0	-	-	3.04	0.056	2.92
24	11/29/81	03 35 08	49.847N	78.852E	5.6	-	-	2.80	0.057	2.76
25	12/27/81	03 43 14	49.923N	78.876E	6.2	-	-	3.11	0.060	3.05

Table VI.6.1 List of events used in this study. The table gives event no., date, origin time, magnitude (m_b) by NEIS, ISC and NORSAR (instrument 01A04), log RMS Lg averaged across NORSAR and the corresponding standard deviation and log RMS Lg measured on instrument 03C01. Note that ISC and NORSAR mb values are not available for all events.

VI.7 A new regional array in Norway: Design work

A prototype regional array will be installed in Norway during the summer of 1984. According to firm plans as of 1 June 1983, the array will comprise 25 short period elements, 4 out of which will be 3-component deployments with the remaining 21 elements consisting of vertical motion seismometers only. In addition, there will be a broad-band three-component system. Sampling rates will be 40 Hz for the short-period channels and 10 Hz for the broad-band system.

The on-line processing of data from the 25 vertical short-period channels will be based on an existing program package (Mykkeltveit et al, 1982; Mykkeltveit and Bungum, 1982). The subject of this contribution is the geometrical configuration of the 25-channel vertical array.

Design experiments

We have previously devised a method for array configuration optimization with respect to SNR gain by beamforming (Mykkeltveit et al, 1983). We have demonstrated optimized geometries leading to theoretical gains well in excess of the standard $\sqrt{N}$ gain, by utilizing negative minima in the observed noise correlation curves. Such optimum geometries, however, tended to be rather 'peaked' in their frequency response, i.e., a very high gain at one particular frequency was generally accompanied by low gains at other (relevant) frequencies. The optimized geometries were characterized by one particular intersensor spacing being represented as many times as possible in the geometry. This distance reflects the separation for which the noise correlation has its minimum, for a given frequency interval. For optimization taking several frequency bands into consideration (e.g., giving equal weight to each of five different frequency bands in the gain expression), again one single intermediate frequency 'dominated' the geometry. For on-line processing of regional events on the new array, signal frequencies in the range 1.5 to 5.0 Hz will be of importance. In this range the distance corresponding to the noise correlation minimum varies by as much as a factor of 3 and optimum geometries for different frequencies

within this range would be vastly different. The configuration to be finally deployed must have many combinations of sensor pairs at optimum separation for any frequency within a fairly wide range.

From the foregoing discussion it follows that we have not been able to make much use of our optimization procedure during the more recent stages of planning for the new array. Rather, a design idea set forth by Followill and Harris of LLNL (Followill and Harris, 1983) has been pursued. They propose a geometry based on concentric rings spaced at log-periodic intervals in radius R, according to the formula:

$$R = R_{min} \cdot \alpha^n , \qquad n = 0,1,2,... \tag{1}$$

Their design includes the deployment of an odd number of elements symmetrically distributed in azimuth, and it has the following attractive features:

- With an odd number of elements in each ring, the corresponding coarray (defined as the set of all intersensor separations, in vector space) pattern has no overlap among its points, i.e., it samples the wavefield in the best possible way, in this respect.
- Designs based on (1) comprise comprehensive subsets of sensors with very different typical intersensor separations, implying that both high-frequency and low-frequency phases could be well enhanced by appropriate subsets of the array.
- The beam patterns for the above designs are favorable, with a narrow main lobe yielding good resolution in phase velocity and azimuth and absence of cumbersome side lobes.

More specifically, the configuration in Fig. VI.7.1, OR13579, was proposed for the new array. It is the realization of (1), with R_{min} = 200 m, α = 2.25, n = 0,1,2,3 and with 3,5,7 and 9 elements in each ring, plus one in the center. This gives an array of aperture about 4.45 km. For high-frequency phases (3 Hz and above) the outer ring does not contribute to the gain and should be omitted during

processing. This leaves an array of aperture 2 km. Similarly, the two inner rings should be masked while processing low-frequency phases.

SNR gains by beamforming for the OR13579 design and relevant sub-geometries of it were checked using correlation curves for signals and noise based on recordings on the NORESS array. Signal and noise correlations were measured in the two bands 1-3 and 3-5 Hz and theoretical gains were computed (Mykkeltveit et al, 1983) for a range of values of R_{min} in (1). For each of the two frequency bands and corresponding full set/subset of sensors, the proposed value of R_{min} (200 m) gives gains close to optimum for this design.

The beam pattern of OR13579 is shown in Fig. VI.7.2a. The narrow main lobe is partly due to the large aperture of 4.45 km of this design. Standard beam pattern computations, however, assume identical signals. In order to evaluate the role of the aperture in a wavenumber resolution context, we compute response patterns incorporating realistic signal correlations, and one example of a resulting beam pattern is shown in Fig. VI.7.2b. As can be seen, the resolution capability of the array is degraded through the widening of the main lobe.

Because of the above concerns about actual resolution capability for a 4.45 km aperture array and several logistic constraints, the decision was made to plan for an aperture of about 3 km for the new array, but at the same time retain the basic ideas underlying the OR13579 design. The new proposed design, OR13579 1984, follows from (1) with R_{min} = 150 m and α = 2.15, yielding an outer ring diameter of 2.985 km.

OR13579 1984 was checked with respect to theoretical gains in the same way as described above for OR13579. For this task, we used noise correlation curves for the frequency bands 1.5-2.5 and 3.5-4.5 Hz in conjunction with the previously derived signal correlation curves for the bands 1-3 and 3-5 Hz, thus making the noise correlation curves more representative for the center frequency in the signal bands.

(This amounts to partly compensating for the strong decay with frequency in the noise spectra.)

Gains for the OR13579 1984 geometry as a function of R_{min} are given in Fig. VI.7.3 for different weighting of frequency bands and different sensor masking schemes. It is found that for the proposed value of 150 m for R_{min} it does not pay to delete the outer ring of 9 elements for the higher frequencies. For the lower frequency range, however, gain improvement is achieved by masking the inner two rings. A general impression from this figure is that one should be able to improve the gain by a slight increase of R_{min} and a corresponding increase in the aperture to close to 4 km, but the net gain from this change would amount to less than 1 dB, which is of minor importance compared to the above considerations on array resolution and logistic implications.

Other geometricl patterns, both previous array realizations (CPO, UBO, LASA) and new concepts, have been investigated along the same lines as above. None of these, however, produced both a beam pattern, a co-array pattern and theoretical gains equal to or better than the Followill and Harris odd-ring designs.

1983 temporary field installations

There will be two experiments during the summer/fall of 1983 to evaluate our current ideas of array design. These experiments are:

1) Temporary deployment of five three-component sets. This experiment is designed to give us the background data for the decision of where to deploy the three-component stations in the 1984 array.
2) Deployment of OR13579 1984 with the exception of 4 instruments in the outer ring. This gives us the opportunity of experimental verification of the potentials of the OR13579 1984 design. There is an option for one reconfiguration of the 21 channels in August 1983.

S. Mykkeltveit

References

Followill, F. and D. Harris (1983): Comments on small aperture aarray array designs. Informal report, Lawrence Livermore National Laboratory.

Mykkeltveit, S., H. Bungum and F. Ringdal (1982): A processing package for on-line analysis of data from small-aperture arrays. NORSAR Semiannual Tech. Summ., 1 October 1981-31 March 1982.

Mykkeltveit, S. and H. Bungum (1982): On-line event detection and location based on NORESS data. NORSAR Semiannual Tech. Summ., 1 April - 30 September 1982.

Mykkeltveit, S., K. Åstebøl, D.J. Doornbos and E.S. Husebye (1983): Seismic array configuration optimization. Bull. Seism. Soc. Am. 73, 173-186.

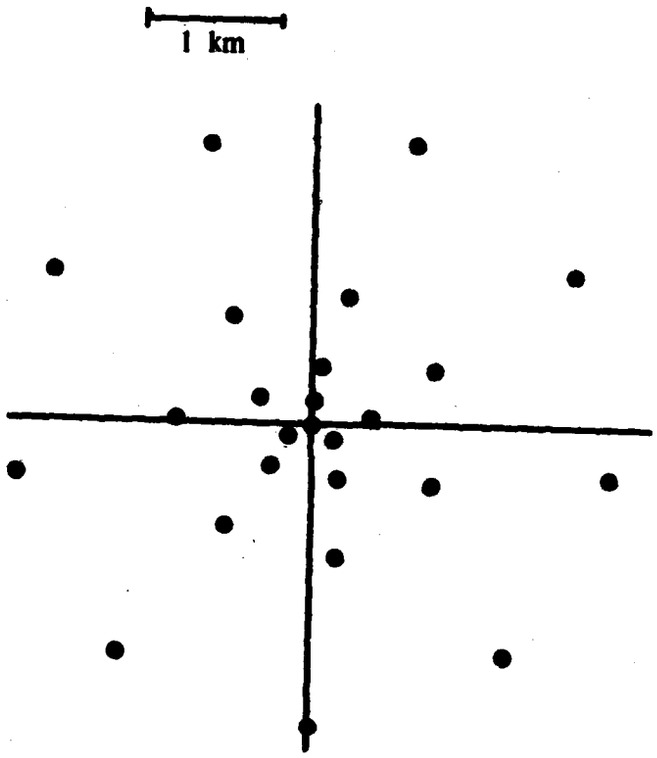

Fig. VI.7.1 Geometry of the OR13579 design by Followill and Harris (1983).

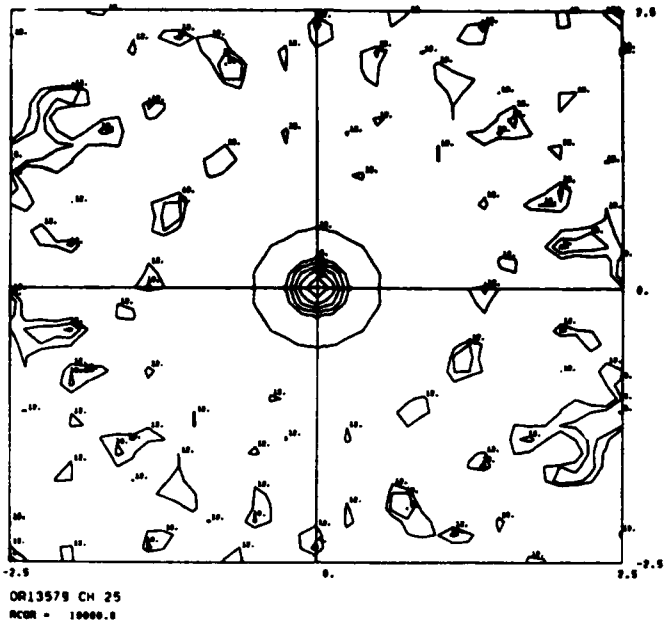

Fig. VI.7.2 (a) Standard beam pattern (impulse and response) for OR13579. This corresponds to signal correlation equal to 1 for all intersensor separations.

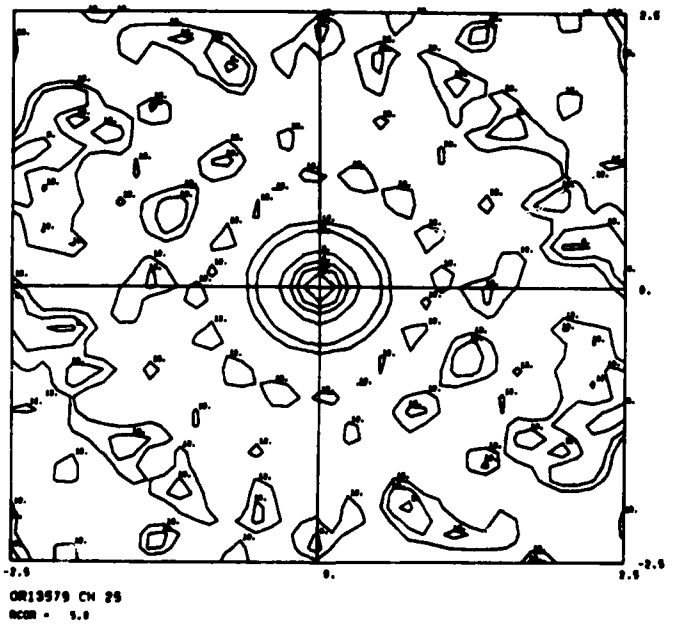

Fig. VI.7.2 (b) Array response for OR13579 for realistic signal correlations. Signal correlation is assumed to be linear and equal to 0 at 5 km intersensor separation. This value is typical of Lg and high-frequency (above ~ 4 Hz) Pn.

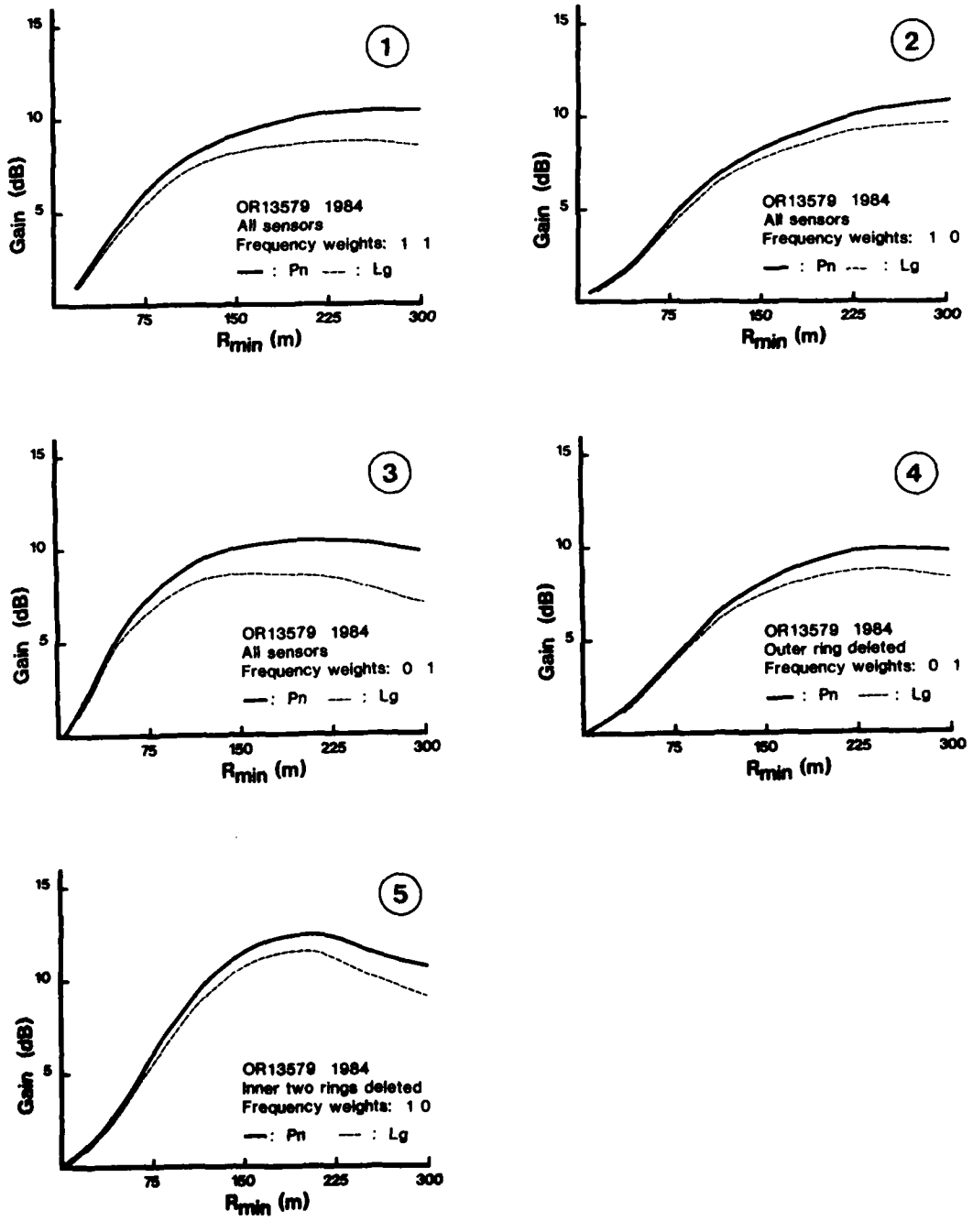

Fig. VI.7.3 Theoretical gains for the OR13579 1984 design and relevant subgeometries, as a function of R_{min}. 'Frequency weights 1 1' means that the low and high frequency bands (1-3 and 3-5 Hz, respectively) are given equal weight in the gain estimation, a.s.o.